Pulsar-black hole binaries: prospects for new gravity tests with future radio telescopes

Kuo Liu, R. P. Eatough, N. Wex, M. Kramer

Monthly Notices
of the
ROYAL ASTRONOMICAL SOCIETY

MNRAS **445,** 3115–3132 (2014) doi:10.1093/mnras/stu1913

Pulsar–black hole binaries: prospects for new gravity tests with future radio telescopes

K. Liu,[1,2,3]★ R. P. Eatough,[3] N. Wex[3] and M. Kramer[3,4]

[1]*Station de radioastronomie de Nançay, Observatoire de Paris, CNRS/INSU, F-18330 Nançay, France*
[2]*Laboratoire de Physique et Chimie de l'Environnement et de l'Espace LPC2E CNRS-Université d'Orléans, F-45071 Orléans Cedex 02, France*
[3]*Max-Planck-Institut für Radioastronomie, Auf dem Hügel 69, D-53121 Bonn, Germany*
[4]*Jodrell Bank Centre for Astrophysics, The University of Manchester, Alan Turing Building, Manchester M13 9PL, UK*

Accepted 2014 September 10. Received 2014 September 10; in original form 2014 July 18

ABSTRACT

The anticipated discovery of a pulsar in orbit with a black hole is expected to provide a unique laboratory for black hole physics and gravity. In this context, the next generation of radio telescopes, like the Five-hundred-meter Aperture Spherical radio Telescope (FAST) and the Square Kilometre Array (SKA), with their unprecedented sensitivity, will play a key role. In this paper, we investigate the capability of future radio telescopes to probe the space–time of a black hole and test gravity theories by timing a pulsar orbiting a stellar-mass black hole (SBH). Based on mock data simulations, we show that a few years of timing observations of a sufficiently compact pulsar–SBH (PSR–SBH) system with future radio telescopes would allow precise measurements of the black hole mass and spin. A measurement precision of 1 per cent can be expected for the spin. Measuring the quadrupole moment of the black hole, needed to test general relativity's (GR's) no-hair theorem, requires extreme system configurations with compact orbits and a large SBH mass. Additionally, we show that a PSR–SBH system can lead to greatly improved constraints on alternative gravity theories even if they predict black holes (practically) identical to GR's. This is demonstrated for a specific class of scalar–tensor theories. Finally, we investigate the requirements for searching for PSR–SBH systems. It is shown that the high sensitivity of the next generation of radio telescopes is key for discovering compact PSR–SBH systems, as it will allow for sufficiently short survey integration times.

Key words: gravitation – pulsars: general.

1 INTRODUCTION

The discovery of the first binary pulsar in 1974 marked the beginning of a completely new field in experimental gravity (Hulse & Taylor 1975). The clock-like nature of pulsars makes relativistic binary pulsar systems ideal test beds of relativistic theories of gravity, i.e. general relativity (GR) and its alternatives (Damour 2009). A system of a pulsar in orbit with a black hole will be a unique celestial laboratory for such tests, by both allowing for qualitatively new tests of gravity and greatly improving the previous results (Kramer et al. 2004). Wex & Kopeikin (1999) first pointed out that pulsar timing can be used to measure the properties of the companion black hole, and test GR's cosmic censorship conjecture and no-hair theorem. It also has been shown that a pulsar–black hole system is a great tool in constraining alternative gravity theories, such as scalar–tensor theories of gravity (Damour & Esposito-Farèse 1998; Esposito-Farèse 2009) and extra spatial dimensions (Simonetti et al. 2011).

Pulsars are usually weak radio sources and the precision of most current tests are still limited by instrumental sensitivity. Therefore, the next generation of radio telescopes, which will provide a significant increase in source flux gain, are ideal tools to carry out the aforementioned experiments. Theoretically, they will provide one to two orders of magnitude improvement in timing precision for millisecond pulsars (MSPs) of normal flux density (Liu et al. 2011). The Square Kilometre Array (SKA) and the Five-hundred-meter Aperture Spherical radio Telescope (FAST) are the two representatives which this paper will mainly refer to. It is certain that the next generation of radio telescopes will open a new era on gravity theory studies, mainly driven by the new pulsar timing and searching capabilities of these future instruments (Kramer et al. 2004; Lazio 2013).

There are mainly two scenarios where a pulsar is in orbit with a black hole: a pulsar and stellar-mass black hole (SBH) binary, and a pulsar moving around a significantly more massive black hole at the centre of either the Galaxy or a globular cluster. Concerning the second scenario, timing experiments and gravity tests with a pulsar in orbit about the supermassive black hole Sgr A★ in the Galactic Centre have already been discussed in detail by Liu et al.

★ E-mail: kliu.psr@googlemail.com

(2012). They show that a few years of timing of a pulsar near Sgr A* (orbital period of a few months) with the SKA should allow for the determination of the black hole mass and spin with high precision (fractional precision of $\sim 10^{-5}$ and $\sim 10^{-3}$, respectively) and may lead to a test of the no-hair theorem with $\lesssim 1$ per cent precision. In this paper, we will mainly focus on the first scenario, a system consisting of a pulsar and an SBH (PSR–SBH system).

An order of $\sim 10^8$ isolated SBHs are estimated to exist in our Galaxy (Shapiro & Teukolsky 1983; van den Heuvel 1992). So far 24 SBHs, as members of X-ray binaries, have been identified via their masses, most of them within our own Galaxy (Narayan & McClintock 2013). The masses found range from about 5 to 30 solar masses. Based on models of the accretion flow, which depends very strongly on how spin affects the strong-field black hole space–time, for several of the SBH candidates the spin parameter χ has been determined. Quite a few of the SBH candidates seem to rotate at a large fraction of the maximum spin ($\chi = 1$), with $\chi > 0.983\,(3\sigma)$ for Cyg X-1 being the largest one (Gou et al. 2011, 2014). So far, for none of the SBH candidates measurements are accurate enough to allow for a test of the no-hair theorem. More details and references for the current SBH candidates are provided by Narayan & McClintock (2013).

There exist a few channels through which a PSR–SBH binary can be formed. The first is to follow the standard binary evolutionary path that has been widely studied by previous works (Yungelson & Portegies Zwart 1998; Voss & Tauris 2003), which may result in a PSR–SBH system of wide and eccentric orbit and a young pulsar with slow spin-periods ($\sim$0.1–1 s). The second approach is a so-called reversal mechanism where under a certain set of circumstances the pulsar is formed first and later spun up by accretion during the red giant phase of the other star (Sipior, Portegies Zwart & Nelemans 2004; Pfahl, Podsiadlowski & Rappaport 2005). This may result in a system consisting of a recycled pulsar in orbit with a black hole, which is more desirable given that recycled pulsars are generally more precise timers than slow 'normal' pulsars (e.g. Verbiest et al. 2009). Thirdly, a PSR–SBH system can be formed through multiple body encounter, which is known to occur in regions of high stellar density, such as globular clusters and the Galactic Centre region (Faucher-Giguère & Loeb 2011; Clausen, Sigurdsson & Chernoff 2014). As a matter of fact, in many globular clusters we already know of several cases, where the pulsar was first fully recycled to have millisecond rotational period in a low-eccentricity binary system with a low-mass companion and later disrupted by the intrusion of a more massive stellar remnant. This normally results in binary MSPs with eccentric orbits and massive companions like M15C (Prince et al. 1991), NGC 1851A (Freire et al. 2004; Freire, Ransom & Gupta 2007) and NGC 6544B (Lynch et al. 2012), and is exactly the same mechanism that is expected to produce an MSP–SBH system in a globular cluster. In this paper, we will not elaborate on the formation scenario or population synthesis of PSR–SBH systems, but focus on the technical requirements and the PSR–SBH system configurations that are necessary for different tests of black hole physics and theories of gravity.

One of the major difficulties in finding PSR–SBH systems is the lack of computational power (Eatough 2009). Nevertheless, recently developed techniques such as the global volunteer distributed computing project Einstein@home[1] have already been involved in finding binary pulsars (Knispel et al. 2010). In addition, the sensitivity of future telescopes will allow us to overcome many of the computational limits imposed by long pointing times through significantly shorter integrations, which will greatly enhance our chance for the discovery of PSR–SBH systems.

The structure of the paper is as follows. In Section 2, we introduce the design of the FAST and the SKA as two representatives of the next generation of radio telescopes, as well as their corresponding achievable timing precisions. In Section 3, we discuss the measurability of black hole properties and tests of GR's cosmic censorship conjecture and the no-hair theorem by timing a PSR–SBH system. Section 4 shows the expected constraints on scalar–tensor theories of gravity by a PSR–SBH system. A discussion on external effects that may influence the aforementioned gravity tests is presented in Section 5. Section 6 demonstrates that the sensitivity allowed by the next generation of radio telescopes would provide a significantly better chance to recover the pulsar signal in a strong gravitational field. Our conclusion is shown in Section 7.

2 INSTRUMENTATION AND TIMING LIMITS WITH FUTURE TELESCOPES

The next generation of radio telescopes will provide an increase in collecting area by a factor of 10–100, compared with the current largest steerable single-dish antennas, and a factor of a few to 25 compared to Arecibo, the current largest single-aperture radio telescope. Ideally, this will translate into the same orders of magnitude improvement in pulsar-timing precision, which would greatly boost the quality of current gravity tests and enable new types of experiment (Kramer et al. 2004).

2.1 Telescope designs

In a few years from now, the FAST will be the largest single-dish radio telescope on Earth (Nan 2006; Nan et al. 2011). FAST is designed as an Arecibo-type antenna and built into a karst depression in southern China, which is sufficiently large to hold the 500-m diameter dish. The effective aperture of FAST is equivalent to a fully illuminated 300-m dish. The main reflector consists of $\sim$4400 triangular elements which allow surface formation from a sphere to a paraboloid in real time via active control. The deep depression and feed cabin suspension system allow a 40° zenith angle, which may be extended later by applying feeding techniques like Phased Array Feeds (PAFs) in an upgrade stage (Nan et al. 2011). An order of magnitude improvement in sensitivity can be expected with FAST compared to a 100-m dish.

The SKA with its collecting area of about 10^6 m^2 currently represents the ultimate design of future radio telescopes (Schilizzi et al. 2007). It will be built in phases, but already SKA Phase 1 will be amongst the largest radio telescopes on Earth, and by far the largest on the Southern hemisphere. The key science of this international project is to address a wide range of questions in astrophysics, fundamental physics, cosmology and particle astrophysics, including gravitational wave astronomy in the nano-Hz band and extreme GR tests including pulsar–black hole binaries.

In the current SKA baseline design, the telescope consists of three parts. For pulsar searches discussed here, the important components are a sparse aperture array (SKA-low) of simple dipole antennas to cover the low-frequency range of 50–350 MHz, and a dish array (SKA-mid) of $\sim$15 m diameter elements to cover the high-frequency range from 350 MHz to 14 GHz. Each of them will concentrate most of the collecting area in a central circular region with diameter of about 5 km. It is mostly this area that can be phased-up for pulsar searches with synthesized beams within the primary field of

[1] http://einstein.phys.uwm.edu/

Table 1. Approximate values of the expected sensitivity (effective collecting area, $A_{\rm eff}$, divided by system temperature, $T_{\rm sys}$) at 1.4 GHz and TOA precision with 10-min integration time $\sigma_{\rm 10\,min}$ for different telescopes used in this paper (Nan et al. 2011; Dewdney et al. 2013). Here, we assume a pulsar of 1 mJy flux density, 5 ms period, and 100 μs pulse width. The observing bandwidth is assumed to be 500 MHz.

	$A_{\rm eff}/T_{\rm sys}$ ($\rm m^2\,K^{-1}$)	$\sigma_{\rm 10\,min}$ (μs)
100-m dish	200	1.0
FAST	2000	0.1
SKA1-mid	1630	0.12
Full SKA-mid	10 000	0.02

view. While SKA1-low is supposed to provide a sensitivity that is somewhat less than that of FAST, SKA1-mid should provide similar sensitivity. The full SKA-mid in Phase II will be equivalent to a telescope with an effective collecting area of about 1 $\rm km^2$, which will enable an ∼50 times improvement in sensitivity at 1.4 GHz compared with a 100-m dish (Schilizzi et al. 2007).

2.2 Expected improvements in pulsar-timing precision

The current timing precision for slow pulsars is limited by irregularities of the pulsar's spin (e.g. Lyne et al. 2010), which is difficult to be improved by an increase in telescope sensitivity. However, the rms timing residuals for most MSPs are still dominated by system white noise (e.g. Verbiest et al. 2009), which can be greatly decreased by the increased instantaneous gain of the future telescopes. Here, following the method in Liu et al. (2011), we estimated the expected measurement precision on pulse time-of-arrivals (TOAs) at 1.4 GHz with the application of the SKA and the FAST, compared with that achievable with a 100-m dish. The results together with the presumed instrumental sensitivities are summarized in Table 1. It can be seen that in an optimal case the full SKA-mid will provide nearly two orders of magnitude improvement to the timing precision. Note that we do not consider intrinsic noise due to profile phase jitter, since first the phenomenon is source dependent (e.g. Jenet et al. 1998; Jenet & Gil 2004), secondly it can be decreased by extending integration time (Cordes & Shannon 2010) and thirdly it may be corrected with potential methods being developed (e.g. Osłowski et al. 2011).

3 TESTING THE PROPERTIES OF A BLACK HOLE SPACE–TIME

As an exact solution to Einstein's field equations of GR, the Kerr metric describes the outer space–time of an astrophysical (uncharged) black hole (e.g. Thorne, Price & Macdonald 1986). At the centre of the black hole lies a gravitational singularity, a region where the curvature of space–time diverges. Penrose's 'Cosmic Censorship Conjecture' states that within GR such singularities are always hidden within the event of horizon (Penrose 1979), giving an upper limit for the black hole spin $S_\bullet$, which is

$$\chi \equiv \frac{c}{G}\frac{S_\bullet}{M_\bullet^2} \leq 1, \tag{1}$$

where c is the speed of light and $M_\bullet$ the mass of the black hole. Therefore, measurements of the black hole mass and spin can be used to test this inequality. A measured χ exceeding unity in a tight pulsar binary system would pose an interesting challenge for our understanding of the nature of the compact pulsar companion, or even call our concept of gravity and space–time into question. Within the Kerr solution, for $\chi > 1$ the event horizon vanishes, indicating the possibility of a space–time singularity being exposed to the outside universe, which is a violation of the cosmic censorship conjecture (Penrose 1979). On the other hand, $\chi > 1$ could signal an extremely unusual object within GR (e.g. Ryan 1997), or even the breakdown of GR itself.

Astrophysical black holes are believed to be results of a gravitational collapse, during which all properties of the progenitor, apart from the mass and spin, are radiated away by gravitational radiation while the gravitational field asymptotically approaches its stationary configuration (Price 1972a,b). Consequently, all higher multipole moments of the gravitational field of an astrophysical black hole can be expressed as a function of $M_\bullet$ and $S_\bullet$, which is the consequence of the 'no-hair theorem' (Hansen 1974). In particular, the quadrupole moment, $Q_\bullet$, fulfills the relation (Thorne 1980)

$$q \equiv \frac{c^4}{G^2}\frac{Q_\bullet}{M_\bullet^3} = -\chi^2, \tag{2}$$

where q is the dimensionless quadruple moment. A measurement of q in a clean system would therefore provide a (model-independent) test of the no-hair theorem for a Kerr black hole. In future, this could be achieved, for instance, through the observations of gravitational waves from the inspiral of a compact object into a massive black hole (Ryan 1995), or the timing observations of a pulsar in a tight orbit around a black hole (Wex & Kopeikin 1999; Kramer et al. 2004; Liu et al. 2012).

Concerning timing observations of a PSR–SBH system, the mass determination can be achieved by measuring a variety of relativistic effects that can be parametrized by a set of post-Keplerian (PK) parameters, just like the previous experiments with binary pulsars (see Lorimer & Kramer 2005, for a detailed summary). For a Kerr black hole, the spin-induced frame dragging will cause the pulsar orbit to precess about the direction of the total angular momentum, which can be properly modelled and used to derive the spin and system geometry. The quadrupolar potential due to the 'oblateness' of the black hole will induce periodic perturbations to the pulsar orbit, which in principle may lead to a measurement of the black hole quadrupole moment.

This section will begin with an extensive discussion on the mass determination for pulsar and black hole, and then investigate in detail the effects of the black hole spin and quadrupole moment on the orbital dynamics of the pulsar and their measurability through pulsar timing.

3.1 Mass measurement

The mass measurement for the black hole is essential in identifying the pulsar companion as a black hole. A well-determined mass that clearly exceeds the maximum mass of a neutron star ($\lesssim 3\,\rm M_\odot$) for any reasonable equation-of-state (EoS), in combination with optical observations[2] that can exclude a main-sequence star, would make a very strong case for the black hole nature of the pulsar companion. In principle, there could be more exotic alternatives to black holes, but many of them are expected to differ in their spin and quadrupole properties, a test where again a precise mass is the key input.

[2] If the pulsar is in a tight orbit around its massive companion, then already the absence of eclipses and tidal effects would argue for a sufficiently compact companion, and consequently for a black hole.

When describing timing observation of relativistic pulsar binary systems, one can use a set of theory-independent PK parameters which, for a given theory of gravity, are theory-specific functions of the two a priori unknown masses (e.g. Damour & Deruelle 1986; Damour & Taylor 1992). Consequently, if measurements of any two PK parameters are achieved, the masses can then be derived assuming GR is correct. The measurement of a third PK parameter would then verify the applicability of GR for the mass determination. In the following, we briefly introduce several such parameters that are commonly used in pulsar timing for mass determinations, and discuss their measurability in PSR–SBH systems, based on mock data simulations. We keep only the leading terms which are sufficient to estimate the measurement precisions, as argued in Liu et al. (2012).

3.1.1 PK parameters and mass determination

In eccentric pulsar binaries, the precession of periastron is usually the first PK parameter that can be measured with high precision. Typically, the major contribution is from the mass monopoles which following Robertson (1938) can be written as

$$\dot{\omega}_{\rm m} = \frac{3}{1-e^2}\left(\frac{P_{\rm b}}{2\pi}\right)^{-5/3} {\rm T}_\odot^{2/3}\,(m_{\rm p}+m_\bullet)^{2/3}, \tag{3}$$

and for $m_\bullet \gtrsim 10$ be approximated by

$$\dot{\omega}_{\rm m} \approx (0.92\,{\rm deg\,yr^{-1}})\,\frac{1}{1-{\rm e}^2}\left(\frac{{\rm P_b}}{1\,{\rm d}}\right)^{-5/3}\left(\frac{{\rm m}_\bullet}{10}\right)^{2/3}, \tag{4}$$

where e is the orbital eccentricity, $P_{\rm b}$ is the orbital period, ${\rm T}_\odot \equiv G{\rm M}_\odot/c^3 \simeq 4.9255\,\mu{\rm s}$ is the solar mass in seconds, $m_{\rm p}$ and $m_\bullet$ are masses of the pulsar and the companion black hole in solar units, respectively. For systems of $m_\bullet > 10$ and $P_{\rm b} < 1$ d, the precession rate is larger than 1 deg yr^{-1}, which after a few years of timing observations would result in a precise measurement of $\dot{\omega}$. However, if the black hole in a PSR–SBH system is fast rotating, a significant fraction of periastron advance can also be induced by frame dragging (Barker & O'Connell 1975). In this case, the observed $\dot{\omega}$ cannot be used directly for a precise mass determination, but is useful in determining the black hole spin and system geometry, which will be shown in Section 3.2.

The *Einstein delay* is a combination of the second-order Doppler effect and gravitational redshift. Its amplitude is also a PK parameter and within GR determined as (Blandford & Teukolsky 1976)

$$\gamma = e\left(\frac{P_{\rm b}}{2\pi}\right)^{1/3} {\rm T}_\odot^{2/3}\,\frac{(m_{\rm p}+2m_\bullet)m_\bullet}{(m_{\rm p}+m_\bullet)^{4/3}}$$

$$\approx (64\,{\rm ms})\,e\left(\frac{P_{\rm b}}{1\,{\rm d}}\right)^{1/3}\left(\frac{m_\bullet}{10}\right)^{2/3},\ \text{for } m_\bullet \gg m_{\rm p}. \tag{5}$$

Clearly, the effect is important only when the system is sufficiently eccentric (e.g. $e \gtrsim 0.1$). For eccentric orbits with $P_{\rm b} \sim 0.1$–1 d and $m_\bullet \gtrsim 10$, γ would be of order $10 \sim 100$ ms, well above the expected timing precision. However, at the beginning of observation the Einstein delay is always degenerate with the Römer delay[3] and is separable only when the relativistic advance of pericentre (see equation 3) changed the orbital orientation by a sufficient amount.

[3] The Römer delay is defined as $\Delta_{\rm R} = \hat{\boldsymbol{K}}_0 \cdot \boldsymbol{r}$, where $\hat{\boldsymbol{K}}_0$ is the unit vector along the l.o.s. to the PSR–SBH system, and $\boldsymbol{r}$ is the position vector of the pulsar with respect to the barycentre of the binary system. It describes the contribution of the pulsar's orbital motion to the signal traveltime.

The *Shapiro delay* accounts for the additional light traveltime due to the curvature of space–time induced by the companion mass. It contains two separately measurable PK parameters, which in GR read

$$r_{\rm Sh} = {\rm T}_\odot m_\bullet, \quad s_{\rm Sh} = \sin i. \tag{6}$$

The angle i is defined as the angle between the line of sight (l.o.s.) and the orbital angular momentum of the binary system. Following Blandford & Teukolsky (1976) and Damour & Deruelle (1986) one finds

$$\Delta_{\rm Sh} = 2\,r_{\rm Sh}\,\ln\left[\frac{1+e\cos\phi}{1-s_{\rm Sh}\sin(\omega+\phi)}\right]$$

$$\simeq (98.5\,\mu{\rm s})\left(\frac{m_\bullet}{10}\right)\ln\left[\frac{1+e\cos\phi}{1-s_{\rm Sh}\sin(\omega+\phi)}\right], \tag{7}$$

where ϕ is the orbital true anomaly. For systems of either significant eccentricity or inclination angle, the signal would be of the order $10 \sim 100$ μs when $m_\bullet \gtrsim 10$. This is still well above the expected timing precision and should allow precise mass measurements. In GR, $\sin i$ is related to $m_{\rm p}$ and $m_\bullet$ by the mass function

$$s_{\rm Sh} \equiv \sin i = x\left(\frac{P_{\rm b}}{2\pi}\right)^{-2/3} {\rm T}_\odot^{-1/3}\,\frac{(m_{\rm p}+m_\bullet)^{2/3}}{m_\bullet}, \tag{8}$$

where x is the projected semimajor axis of the pulsar orbit measured in light-seconds, i.e. $x \equiv a_{\rm p}\sin i/c$.

The change in orbital period is an additional PK parameter directly measurable from pulsar timing. In GR, the quadrupole radiation predicts (e.g. Peters 1964)

$$\dot{P}_{\rm b} = -\frac{192\pi}{5}\left(\frac{P_{\rm b}}{2\pi}\right)^{-5/3} {\rm T}_\odot^{5/3}\,\frac{m_{\rm p}m_\bullet}{(m_{\rm p}+m_\bullet)^{1/3}}\,f(e), \tag{9}$$

where

$$f(e) = \frac{1+(73/24)e^2+(37/96)e^4}{(1-e^2)^{7/2}}. \tag{10}$$

For $m_\bullet \gtrsim 10$ and $m_{\rm p} \approx 1.4$ one has

$$\dot{P}_{\rm b} \approx (-4.5\,\mu{\rm s\,yr^{-1}})\left(\frac{P_{\rm b}}{1\,{\rm d}}\right)^{-5/3}\left(\frac{m_\bullet}{10}\right)^{5/3} f(e). \tag{11}$$

Consequently, in PSR–SBH systems with short orbital periods (∼1 d), $\dot{P}_{\rm b}$ should be measurable with high precision after only a few years of timing observations.

3.1.2 Mock data analysis

The measurability of the PK parameters in PSR–SBH systems has been investigated based on simulated timing data. The simulations performed in this paper mainly contain two steps. First, based on presumed observing scheme, the TOAs are generated regularly regarding to pulsar's initial time and then combined with the three time delays (Römer, Einstein and Shapiro) to account for the changes in the signal arrival time at the barycentre due to the pulsar's orbital motion. Next, the simulated TOAs are passed to the TEMPO software package, which, based on a timing model, performs a least-squares fit to yield a phase-connected solution of the TOAs, and determines the timing model parameters. The measurement uncertainties of these parameters are produced from the covariance matrix. In this subsection, we used the DD timing model (Damour & Deruelle 1986) to obtain the following results.

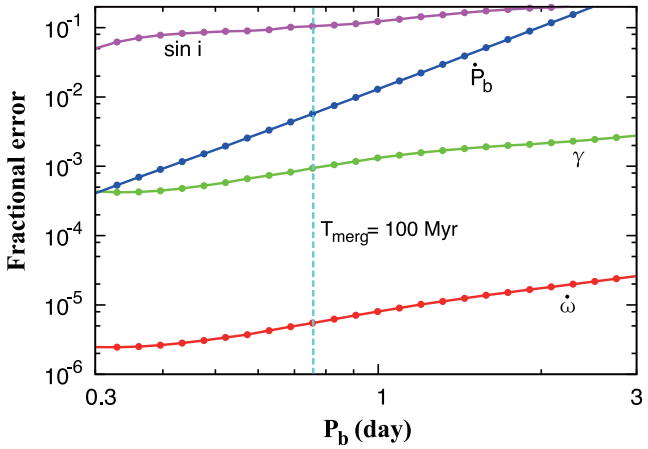

Figure 1. Simulated fractional measurement errors of PK parameters as a function of P_b for PSR–SBH systems of a slow pulsar. The assumed system parameters are: $e = 0.8$, $m_p = 1.4$, $m_\bullet = 10$, $i = 60°$. Here, we assume 10 TOAs per week of 100 μs precision for timing observation with 5-yr baseline. The simulation is carried out for non-rotating black holes.

In Fig. 1, we present expected measurement precisions of the PK parameters from PSR–SBH systems where the pulsar is non-recycled. Here, as mentioned in Section 1, the orbit is likely to be highly eccentric. Note that the timing precision of slow pulsars are normally dominated by timing noise and thus not expected to be significantly improved by system sensitivity (e.g. Lyne et al. 2010). Accordingly, we assumed 5-yr observations leading to 10 TOAs per week with a precision of 100 μs. To indicate systems with a realistic lifetime, we label the orbital period corresponding to a gravitational merging time-scale of 100 Myr, the value of the most relativistic (currently known) binary pulsar system PSR J0737−3039. The merging time-scale is given by (e.g. Peters 1964)

$$T_{\rm merg} = \frac{5}{256}\left(\frac{P_{\rm b}}{2\pi}\right)^{8/3} {\rm T}_\odot^{-5/3} \frac{(m_{\rm p}+m_\bullet)^{1/3}}{m_{\rm p} m_\bullet}\, g(e), \qquad (12)$$

where

$$g(e) = 1 - 3.6481\, e^2 + 5.1237\, e^4 - 3.5427\, e^6 + 1.3124\, e^8 - 0.2453\, e^{10} \qquad (13)$$

represents an approximation to the corresponding integral in equation 5.14 of Peters (1964), with a <1 per cent fractional error for $e \leq 0.9$. For $m_\bullet \gtrsim 10$ and $m_{\rm p} \approx 1.4$ one finds

$$T_{\rm merg} \approx (725\,{\rm Myr}) \left(\frac{P_{\rm b}}{1\,{\rm d}}\right)^{8/3} \left(\frac{m_\bullet}{10}\right)^{-2/3} g(e). \qquad (14)$$

It can be seen that after 5 yr of observation, the masses can be obtained with high precision if the orbital period is of a few days or less. The measurable PK parameters are most likely to be $\dot{\omega}$, γ, and $\dot{P}_b$.

In Fig. 2, we consider PK parameter measurements for PSR–SBH systems with an MSP. Here, we applied 4-h observations per week with the sensitivity of a 100-m dish (top), the FAST (middle) and SKA (bottom), which can be converted into 10 TOAs with precision of 1 μs, 100 ns and 20 ns, respectively. The timing baselines were assumed to be 5 yr for the 100-m dish and 3 yr for the future telescopes. It is shown that with the sensitivity of a current 100-m dish after 5 yr of observation the masses are likely to be measured with precision better than 1 per cent. The measurement precision

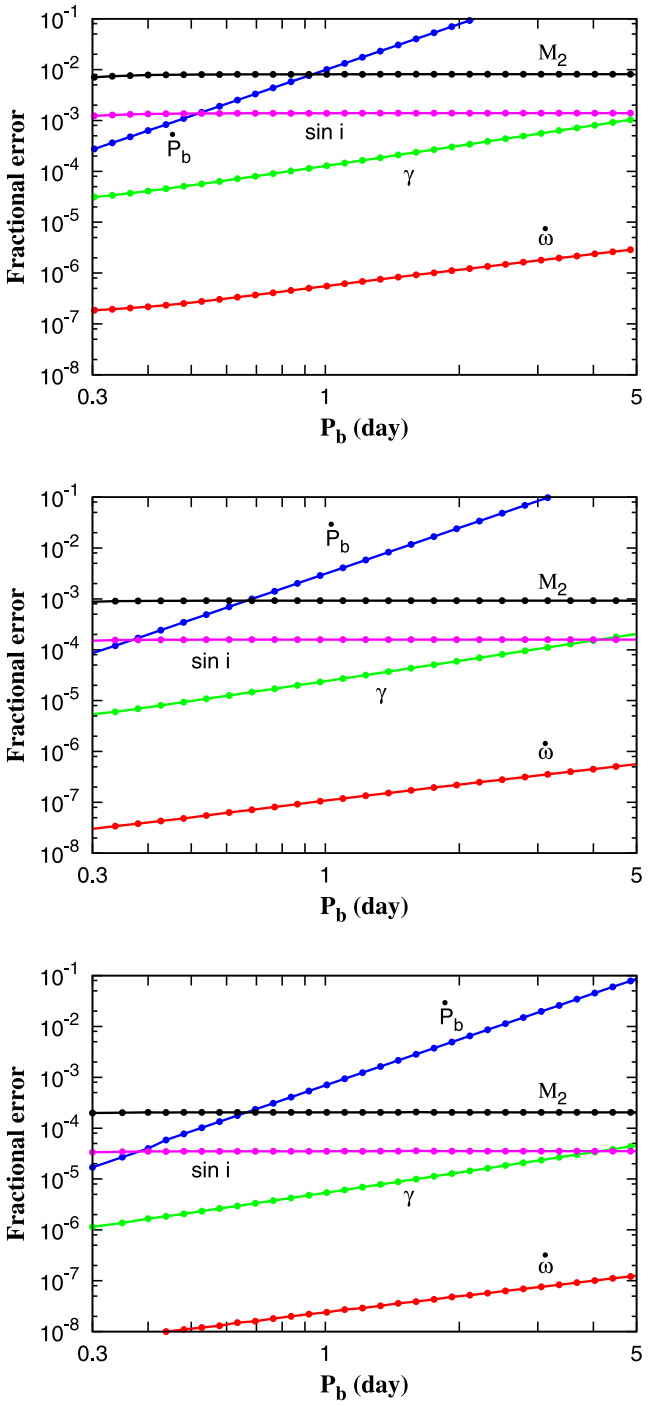

Figure 2. Simulated fractional measurement errors of PK parameters as a function of P_b for PSR–SBH systems with an MSP. Here, we use $e = 0.1$, $m_p = 1.4$, $m_\bullet = 10$, $i = 60°$. Weekly 4 h timing observations are assumed, for 5 yr long (top plot) with a 100-m dish and for 3 yr long (middle plot for the FAST, bottom plot for the SKA) for the future telescopes.

is expected to be improved by a factor of 10–100 with the next generation of radio telescopes.

Note that in Fig. 2 we used a low eccentricity of $e = 0.1$. If a more eccentric system is found, given the same orbital period, the relativistic effects would be stronger thus measured with better precision. In addition, as indicated from equation (7), the measurability

of the Shapiro delay parameters are not significantly dependent on the orbital period. Thus, their measurements would enable mass determination for systems of wide orbits (e.g. $P_b \sim 100$ d). In either case, the periastron advance is well measured but as mentioned in Section 3.1.1, can be directly used for mass measurements only when the black hole is not significantly spinning or the orbit is sufficiently wide.

3.2 Frame dragging, spin measurement and cosmic censorship conjecture

In a binary system, additional to the orbital precession induced by mass monopoles, the spin of the bodies will drag the space–time in the vicinity and cause an extra precession to the orbit (Lense & Thirring 1918; Wex 1995). It was demonstrated by Wex & Kopeikin (1999) that in a PSR–SBH system, the orbital precession can be measured through pulsar-timing observations, and used to determine the black hole spin. In this subsection, we will present a brief description of this effect, and based on mock data simulations, investigate the measurability of the black hole spin and test of the cosmic censorship conjecture with the next generation of radio telescopes.

3.2.1 Orbital precession and its consequence on timing

The precession due to frame dragging can be best described in a coordinate based on the invariant plane perpendicular to the total angular momentum $\boldsymbol{J}$, as shown in Fig. 3. In general, $\boldsymbol{J}$ can be considered as a conserved quantity and both the orbital angular momentum, $\boldsymbol{L}$, and the black hole spin, $\boldsymbol{S}$, are supposed to precess around $\boldsymbol{J}$. Their absolute values are also conserved, if averaged over a whole orbital period. Following Barker & O'Connell (1975) one finds the orbit-averaged frame-dragging precession rate in the form

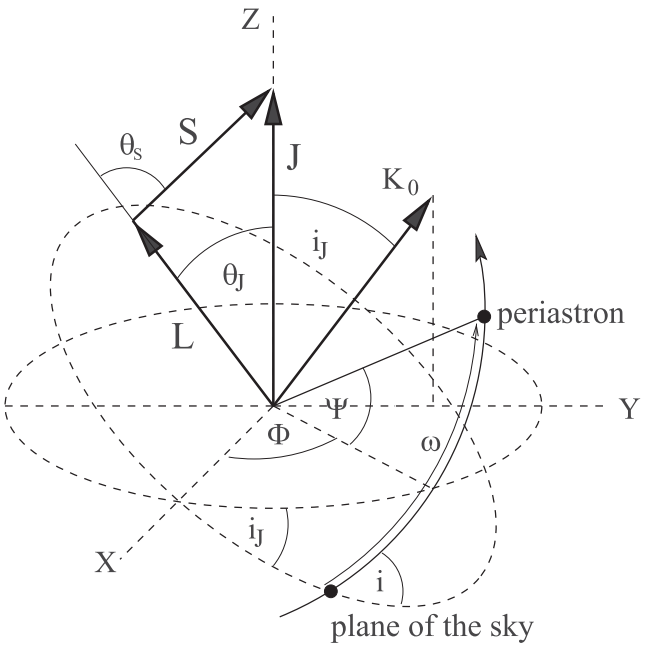

Figure 3. Geometry of a PSR–SBH system. The reference frame is based on the invariable plane perpendicular to the system total angular momentum $\boldsymbol{J}$. The l.o.s. vector $\boldsymbol{K}_0$ is fixed to the Y–Z plane, while the orbital momentum $\boldsymbol{L}$ is supposed to precess around $\boldsymbol{J}$. The definition of angle θ_S, i_J, Φ and Ψ will present a full description of the orbital geometry. The corresponding defined ranges are: $\theta_S, \theta_J, i_J, i \in [0, \pi)$ and $\Phi, \Psi, \omega \in [0, 2\pi)$.

of

$$\dot{\Phi}_S = +\Omega_S^* \frac{\sin\theta_S}{\sin\theta_J}, \tag{15}$$

$$\dot{\Psi}_S = -\Omega_S^* (2\cos\theta_S + \sin\theta_S \cot\theta_J), \tag{16}$$

where

$$\Omega_S^* = \frac{\chi}{(1-e^2)^{3/2}} \left(\frac{2\pi}{P_b}\right)^2 T_\odot \frac{(3m_p + 4m_\bullet)m_\bullet}{2(m_p + m_\bullet)}. \tag{17}$$

For $m_\bullet \gtrsim 10$ and $m_p \approx 1.4$ one finds the following approximate expression:

$$\Omega_S^* \approx (4.4 \times 10^{-3}\,\mathrm{deg\,yr^{-1}}) \frac{\chi}{(1-e^2)^{3/2}} \left(\frac{P_b}{1\,\mathrm{d}}\right)^{-2} \left(\frac{m_\bullet}{10}\right). \tag{18}$$

The linear-in-time secular changes in Φ and Ψ induce non-linear-in-time evolution in two timing parameters, the longitude of periastron ω and projected semimajor axis x. In real timing observations, the variations can be approximated by Taylor expansions as below:

$$x = x_0 + \dot{x}_0(t - T_0) + \frac{1}{2}\ddot{x}_0(t - T_0)^2 + \ldots, \tag{19}$$

$$\omega = \omega_0 + \dot{\omega}_0(t - T_0) + \frac{1}{2}\ddot{\omega}_0(t - T_0)^2 + \ldots, \tag{20}$$

where T_0 is the time of periastron passage and x_0, ω_0 denote the initial values at T_0. As mentioned in Section 3.1.1, the observed $\dot{\omega}_0$ would have a significant contribution caused by the mass monopoles. The contribution by frame dragging can be determined by calculating the monopole component from mass measurements by the other PK parameters and subtract it from the observed $\dot{\omega}_0$.

The contributions to the first and second derivatives, arising from the frame dragging of the black hole companion, have been worked out in detail by Wex & Kopeikin (1999):[4]

$$\dot{x}_S \simeq -x_0\,\chi\,\tilde{\Omega}\,\cot i\,\sin\theta_S \sin\Phi_0, \tag{21}$$

$$\ddot{x}_S \simeq -x_0\,\chi\,\tilde{\Omega}^2\,\tilde{\Sigma}^{-1}\cot i\,\sin\theta_S\cos\Phi_0, \tag{22}$$

$$\dot{\omega}_S \simeq -\chi\,\tilde{\Omega}\,(2\cos\theta_S + \cot i\,\sin\theta_S\cos\Phi_0), \tag{23}$$

$$\ddot{\omega}_S \simeq +\chi\,\tilde{\Omega}^2\,\tilde{\Sigma}^{-1}\cot i\,\sin\theta_S\sin\Phi_0, \tag{24}$$

where

$$\tilde{\Omega} \equiv \Omega_S^*/\chi \tag{25}$$

corresponds to Ω_S^* of an extreme Kerr black hole ($\chi = 1$), and

$$\tilde{\Sigma} \equiv \frac{S_\bullet/\chi}{L} = \left(\frac{P_b}{2\pi}\right)^{-1/3} T_\odot^{1/3} \frac{(m_p + m_\bullet)^{1/3} m_\bullet}{m_p(1-e^2)^{1/2}}. \tag{26}$$

For $m_\bullet \gtrsim 10$ and $m_p \approx 1.4$, one finds

$$\tilde{\Sigma} \approx 0.017 \left(\frac{P_b}{1\,\mathrm{d}}\right)^{-1/3} \left(\frac{m_\bullet}{10}\right)^{4/3}. \tag{27}$$

[4] In equation 64 of Wex & Kopeikin (1999) there is a sign error, Ω_S^* has to be replaced by $-\Omega_S^*$.

Therefore, once these four derivatives are measured, they can then be used to derive χ, θ_S, Φ_0 via equations (21)–(24),[5] which gives the spin amplitude χ and orientation θ_S as

$$\chi \simeq \frac{1}{x_0\tilde{\Omega}}\left[\left(\frac{\Xi_S - x_0\dot{\omega}_S}{2}\right)^2 + \left(\dot{x}_S^2 + \Xi_S^2\right)\tan^2 i\right]^{1/2} \quad (28)$$

and

$$\cos\theta_S \simeq \frac{\Xi_S - x_0\dot{\omega}_S}{\left[(\Xi_S - x_0\dot{\omega}_S)^2 + 4(\dot{x}_S^2 + \Xi_S^2)\tan^2 i\right]^{1/2}} \quad (29)$$

respectively, where

$$\Xi_S \equiv \ddot{x}_S\tilde{\Sigma}/\tilde{\Omega}. \quad (30)$$

θ_S is uniquely determined from $\cos\theta_S$ with the given range of 0–π. Once the spin is determined, the angles in Fig. 3 are all known at the same time. The $i \leftrightarrow \pi - i$ ambiguity from $\sin i$ leads to two different solutions in the orientation by $(\Phi_0, i_J) \leftrightarrow (\pi + \Phi_0, \pi - i_J)$.

3.2.2 *Mock data analysis*

Based on the simulation scheme described in Section 3.1.2, we have estimated the measurability of the black hole spin by timing a PSR–SBH system. Here, when calculating the time delays we also include the orbital precession due to the black hole spin, by inputting the secular changes of Φ and Ψ described in equations (15)–(16). Then, we fit the calculated TOAs with the MSS timing model of TEMPO (Wex 1998) to determine the black hole spin and its orientation, as described in Liu et al. (2012).

The expected black hole spin measurement precision in PSR–SBH systems of a slow pulsar is investigated in Fig. 4. Here, we also show the measurability of the secular change in orbital projected semimajor axis (top), which usually provides the first sign of the black hole spin. We applied the same weekly observing scheme as described in Fig. 1, but extend the timing baseline to 10 yr. The results suggest that by timing a slow pulsar for 10 yr, the spin determination is achievable for a wide range of $m_\bullet$ and χ only if the orbit is compact enough ($P_b \lesssim 0.5$ d) and highly eccentric ($e \gtrsim 0.8$). In wide orbits ($P_b \gtrsim 1$ d), the measurement can be achieved only if the black hole is comparably more massive and fast rotating. Nevertheless, the sign of the frame-dragging effect ($\dot{x}$) can be noticed for a wide range of BH masses and spins when $P_b \lesssim 1$ d.

In Fig. 5, we consider the spin measurement in a PSR–SBH system with an MSP. The observations were based on the same weekly scheme as in Fig. 2, but with baseline of 10 yr for a 100-m dish sensitivity (top plot) and 5 yr for the future telescope level (middle plot for the FAST, bottom plot for the SKA). Clearly, the timing precision with a 100-m dish would allow a black hole spin measurement only when the orbit is compact enough ($P_b \lesssim 0.5$ d). The observations conducted by the future telescopes, on the contrary, would achieve the measurement with precision of order ~1 per cent in only 5 yr for systems with wide ranges in both black hole mass and spin. Note that here we use a low eccentricity of $e = 0.1$ for the orbit. If the pulsar is found to be a more eccentric binary, the spin is even expected to be measurable for systems of orbital period up to ~10 d.

[5] Note that $\dot{x}_S$ and $\dot{\omega}_S$ have the same dependency on spin and system geometry. Here, we use $\dot{x}_S$ since it is generally measured with much higher precision, as will be shown in Section 3.2.2.

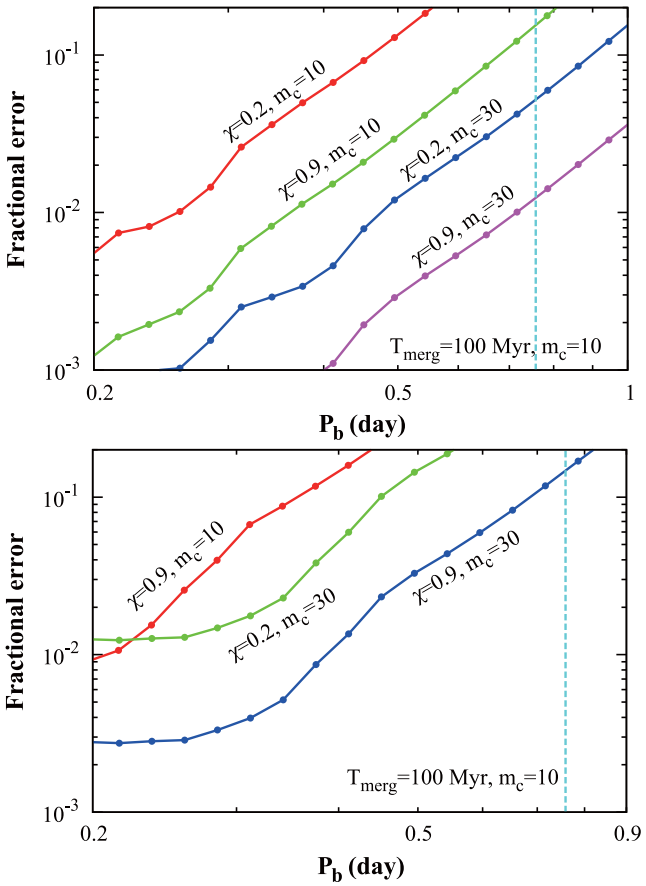

Figure 4. Simulated fractional measurement errors of the frame-dragging effect as a function of orbital period for PSR–SBH systems with a slow pulsar and a 10 and 30 $M_\odot$ BH. The system parameters are: $e = 0.8$, $m_p = 1.4$, $\theta_S = \Phi_0 = 45°$, $i = \Psi_0 = 60°$. Here, we apply the same weekly observational scheme as in Fig. 1, with a baseline of 10 yr. The top plot shows the measurement precision of secular change in orbital projected semimajor axis, the first sign for the existence of black hole spin. The bottom plot presents the measurability of the spin magnitude.

3.3 Quadrupole moment and no-hair theorem

The quadrupole moment of the black hole induces a secular precession of the pulsar orbit which is a few orders of magnitude smaller than the spin contribution and thus is unlikely to be separable from the overall precession (Wex & Kopeikin 1999). Fortunately, the pulsar orbit also endures periodic perturbation by the quadrupolar field of the black hole. As will be shown in this subsection, once the spin magnitude and orientation have been determined by the overall precession of the orbit, in principle this perturbation can be modelled in pulsar timing which might lead to a determination of the black hole quadrupole moment.

3.3.1 *Modulation of the orbital motion and extraction of quadrupole*

The influence of the black hole quadrupole on pulsar's motion leads to a variation in the Römer delay, which can be described by a change in the coordinate position of the pulsar $\boldsymbol{r}'$, described by

$$\boldsymbol{r}' = (r + \delta r^{(q)})(\hat{\boldsymbol{n}} + \delta\hat{\boldsymbol{n}}^{(q)}). \quad (31)$$

The δ-quantities can be derived by following Garfinkel (1958) and Garfinkel (1959), with slight modifications that account for

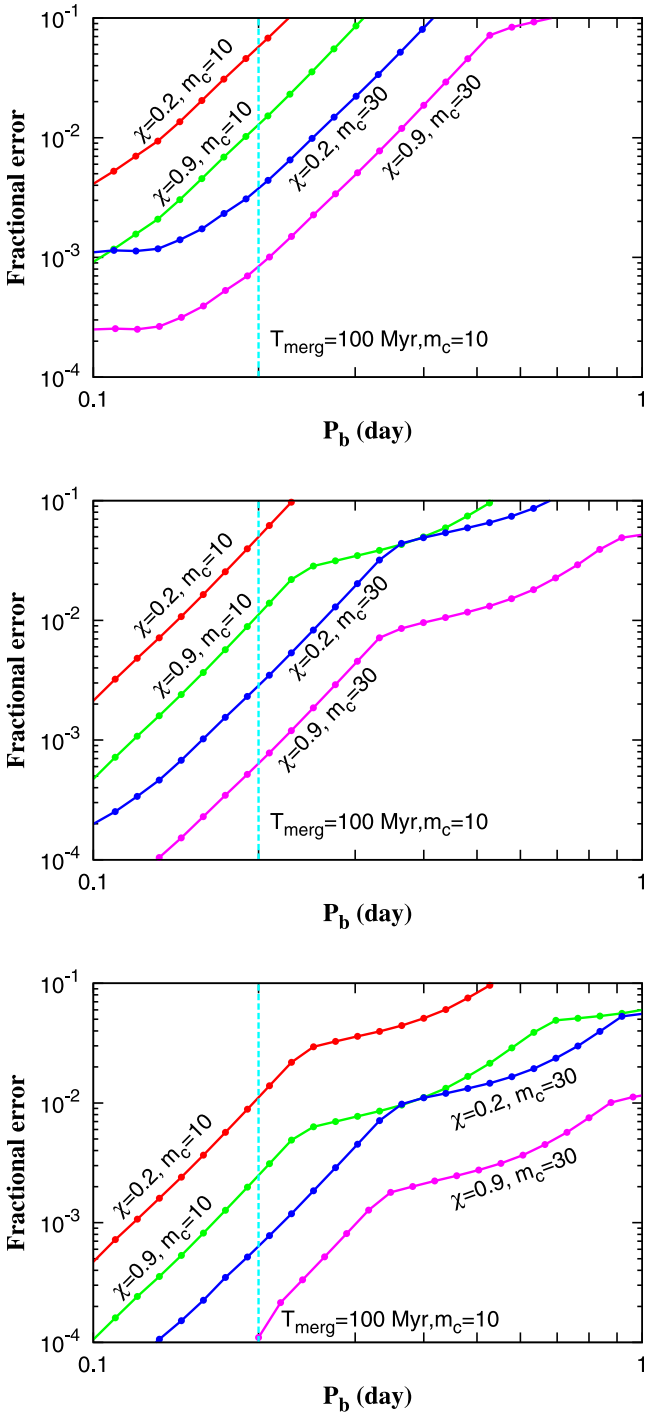

Figure 5. Simulated fractional measurement errors of black hole spin as a function of orbital period for PSR–SBH systems with an MSP. Here the system parameters are: $e = 0.1, m_p = 1.4, \theta_S = \Phi_0 = 45^\circ, i = \Psi_0 = 60^\circ$. For the BH mass, we assume 10 and 30 $M_\odot$. The observations were assumed to be of the same weekly scheme as in Fig. 2, with baseline of 10 yr for a 100-m dish sensitivity in the top plot and 5 yr for the future telescopes sensitivity in the middle (FAST) and bottom (SKA) plot.

the dominating precession of the periastron caused by the mass monopole (for more details, see Liu et al. 2012). The variation scale is proportional to a small dimensionless quantity ϵ which is linked to the black hole quadrupole $Q_\bullet$ by $\epsilon \equiv -3Q_\bullet/a^2(1-e^2)^2$ (Garfinkel 1958; Thorne et al. 1986). Here, a is the orbital semimajor axis. The full expression of the Römer delay can then be expanded with respect to ϵ as

$$\Delta_R = \Delta_R^{(0)} + \delta\Delta_R + \mathcal{O}(\epsilon^2), \tag{32}$$

where $\delta\Delta_R$ is of order ϵ. Based on this approximation as well as the MSS model, a new timing model has been developed that includes the contribution of the black hole quadrupole to first order in ϵ (Liu 2012).

3.3.2 *Mock data analysis*

As first suggested in Wex & Kopeikin (1999), in a PSR–SBH system measurement of the black hole quadrupole moment may not be possible since the amplitude of the quadrupolar signal in one orbital period is only of order $1 \sim 10$ ns even for a highly relativistic system (e.g. $P_b \sim 0.1$ d, $e = 0.9$). Nevertheless, due to the precession of the orbit the quadrupolar feature will evolve on time-scales of years, which can increase the chance to detect the signal. To investigate the circumstances where measurement of the black hole quadrupole moment may become possible, we have performed extensive mock data simulations. We assume weekly, 4 h timing observations of an MSP, for a period of 20 yr with the sensitivity of the SKA. We extend our TOA calculation and use the timing model as described in in Section 3.3.1 to account for the orbital periodic effects due to the black hole quadrupole moment.

As indicated in Wex (1998) and Wex & Kopeikin (1999), in high-eccentricity orbits the quadrupole moment results in strong and sharp features in timing residuals near the orbital periastron. The existence of such features in the timing residuals would benefit the measurement of the quadrupole moment, as shown in Fig. 6. Here, we assume systems of an MSP with a 30 $M_\odot$ black hole, binary merging time of 10 Myr, and three different spin inclinations with respect to the l.o.s. Clearly, the quadrupole moment is measurable only for systems of high eccentricity ($e \gtrsim 0.8$) and favourable geometry (e.g. $20^\circ < \theta_S < 70^\circ$).

The mass of an SBH is usually found to be within the range of $5 \sim 30\,M_\odot$ (Silverman & Filippenko 2008; Ziółkowski 2008).

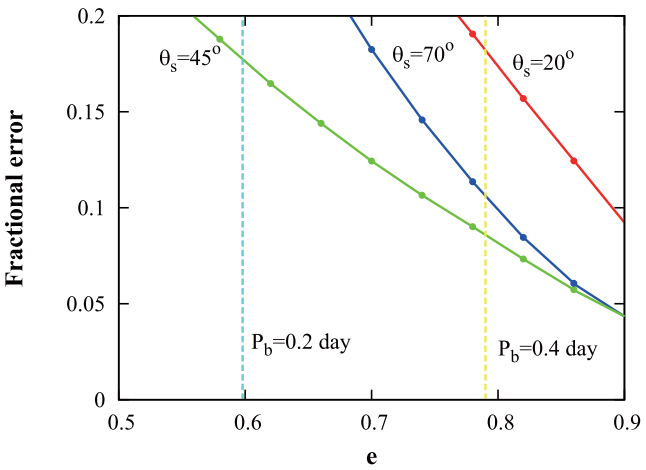

Figure 6. Measurability of the quadrupole moment as function of orbital eccentricity for PSR–SBH systems with a 30 $M_\odot$ black hole, a merger time of 10 Myr and different spin inclination angles θ_S. Here, we assume 20 yr of observations of an MSP with the SKA based on the weekly observing scheme mentioned in Fig. 2. The eccentricity is varied from 0.5 to 0.9 which corresponds to an orbital period range of 0.16 and 0.88 d. The other system parameters are the same as in Fig. 5.

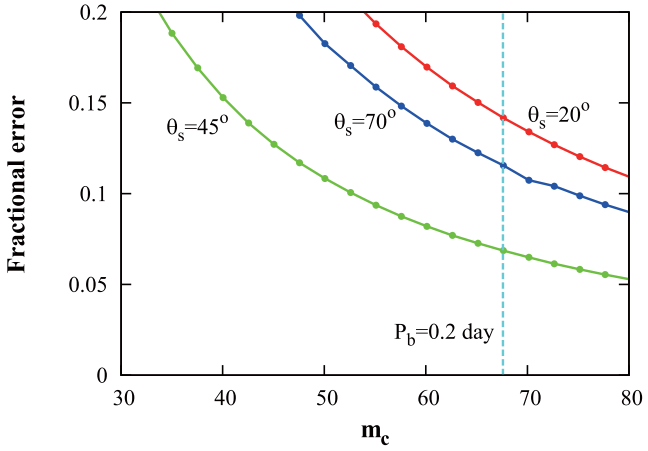

Figure 7. Measurability of the quadrupole moment as function of black hole mass for a 10 Myr lifetime and mildly eccentric ($e = 0.5$) PSR–SBH system, with different spin inclination angles θ_S. Note that the corresponding range of P_b is from 0.16 d (left) to 0.21 d (right). The other system parameters are the same as in Fig. 5. Here again, we assume 20 yr observations of an MSP with the SKA based on the weekly observing scheme mentioned in Fig. 2.

Recent studies have shown that stars with very low metallicity can form SBHs with mass up to 80 $M_\odot$ from direct collapse (Belczynski et al. 2010). Those high-mass SBHs are most likely to be found in regions of very metal-poor environments, such as globular clusters where frequent dynamic captures and 3-body interactions due to the high stellar density might also allow formation of an MSP–SBH system. Note that the quadrupolar field is proportional to the cube of the black hole mass, therefore PSR–SBH systems with a high-mass black hole would undoubtedly benefit the measurement of quadrupole moment. Consequently, for simulations in Fig. 7, while using $e = 0.5$, $T_{\rm merge} = 10$ Myr and three different spin inclinations, we extend the parameter space of $m_\bullet$ to 80, the upper bound given by the current formation studies (Belczynski et al. 2010). The results show that only when $m_\bullet \gtrsim 70$ and there is a favourable geometry (e.g. $20^\circ < \theta_S < 70^\circ$), there is a chance to measure the quadrupole moment of the BH. Therefore, the measurement of the quadrupole moment is possible if one finds a pulsar in orbit with an intermediate mass black hole (IMBH), where $m_\bullet \sim 10^2$–10^4, for instance in the centre of a globular cluster. While there are some promising candidates for IMBH, their existence is still a matter of debate (Narayan & McClintock 2013).

4 TESTING SCALAR–TENSOR GRAVITY WITH PULSAR–BLACK HOLE SYSTEMS

In the previous section we have discussed in detail, how timing a pulsar in orbit with an SBH can be used to probe the properties of a black hole space–time. Questions like 'Is the frame dragging in agreement with a Kerr solution, i.e. $\chi \leq 1$?' and 'Does the quadrupole moment obey the relation given by equation (2) ?' lie at the heart of these experiments. These tests of GR's cosmic censorship conjecture and no-hair theorem with a PSR–SBH system, if in agreement with GR, will at the same time provide constraints on alternative theories of gravity that do not allow for the Kerr solution as the outer space–time of astrophysical black holes. But even for alternatives to GR that also have the Kerr metric as a solution for rotating black holes, e.g. the scalar–tensor theories of Damour & Esposito-Farèse (1992, 1993), a PSR–SBH system would still be an effective test-bed, especially with the sensitivity provided by the next generation of radio telescopes. Like in Wex et al. (2013),[6] we will demonstrate this within the class of quadratic mono-scalar–tensor theories, as introduced by Damour & Esposito-Farèse (1993, 1996), where the gravitational interaction is mediated by a symmetric rank-2 tensor field $g^*_{\mu\nu}$ and a scalar field φ. In the Einstein frame, the field equations read

$$R^*_{\mu\nu} = \frac{8\pi G_*}{c^4}\left(T^*_{\mu\nu} - \frac{1}{2}T^* g^*_{\mu\nu}\right) + 2\partial_\mu\varphi\partial_\nu\varphi, \tag{33}$$

$$g^{\mu\nu}_* \nabla^*_\mu \nabla^*_\nu \varphi = -\frac{4\pi G_*}{c^4}\alpha(\varphi)\, T^*, \tag{34}$$

where $g^*_{\mu\nu}$, $R^*_{\mu\nu}$, $T^*_{\mu\nu}$ and T^* are the metric tensor, the Ricci tensor, the stress–energy tensor and the trace of the stress–energy tensor, respectively, expressed in the Einstein frame (indicated by *). The constant G_* denotes the bare gravitational constant. The physical (Jordan frame) metric $g_{\mu\nu}$ is conformally related to the metric of the Einstein frame $g^*_{\mu\nu}$ by

$$g_{\mu\nu} = e^{2a(\varphi)}\, g^*_{\mu\nu}, \tag{35}$$

and the coupling strength $\alpha(\varphi)$ between the scalar field and matter (see equation 34) is calculated according to

$$\alpha(\varphi) = \partial a(\varphi)/\partial\varphi. \tag{36}$$

In the class of quadratic mono-scalar–tensor theories of Damour & Esposito-Farèse (1993, 1996), denoted as $T_1(\alpha_0, \beta_0)$ by Damour (2009), one has

$$a(\varphi) = \alpha_0(\varphi - \varphi_0) + \frac{1}{2}\beta_0(\varphi - \varphi_0)^2 \tag{37}$$

and

$$\alpha(\varphi) = \alpha_0 + \beta_0(\varphi - \varphi_0), \tag{38}$$

with the two fundamental constants α_0 and β_0. The quantity φ_0 denotes the asymptotic value of φ at spatial infinity. Without loss of generality, here we set $\varphi_0 = 0$. In the weak-field limit ($\varphi \simeq \varphi_0$), α_0 and β_0 give the strength of the linear and quadratic coupling of φ to matter, respectively. Jordan–Fierz–Brans–Dicke gravity is equivalent to the special case $\beta_0 \equiv 0$, and the Brans–Dicke parameter is given by

$$\omega_{\rm BD} = \frac{1}{2}\left(\frac{1}{\alpha_0^2} - 3\right). \tag{39}$$

For a strongly self-gravitating body, like a pulsar, the coupling α_0 has to be replaced by an effective (body-dependent) coupling strength, which is defined as

$$\alpha_{\rm p} \equiv \frac{\partial \ln M_{\rm p}}{\partial\varphi_a}, \tag{40}$$

where φ_a is the asymptotic field felt by the pulsar. Furthermore, in binary pulsar experiments one needs the scalar-field derivative of the effective coupling strength, i.e.

$$\beta_{\rm p} \equiv \frac{\partial\alpha_{\rm p}}{\partial\varphi_a}. \tag{41}$$

The two derivatives above have to be taken for fixed values of the baryonic mass of the pulsar.

Due to their large asymmetry in compactness, binaries of a pulsar and a white dwarf ($\alpha_{\rm WD} \simeq \alpha_0$) are particularly interesting for constraining scalar–tensor theories of gravity, as these systems should

[6] Here we will present the details of the calculation, which we could not in Wex et al. (2013) because of the page limit, and use a more realistic EoS.

lose orbital energy at a much higher rate due to the emission of dipolar gravitational waves (Will 1993; Damour & Esposito-Farèse 1996). A combination of such experiments along with Solar system tests has already placed tight constraints on the (α_0, β_0) parameter space (see Fig. 7 in Freire et al. 2012). In brief, the area $|\alpha_0| > 0.003$ and $\beta_0 < -4.5$ is already excluded. The discovery of a massive pulsar ($m_\mathrm{p} \simeq 2.0\,\mathrm{M}_\odot$) in a relativistic orbit added further restrictions, in particular giving $\beta_0 \gtrsim -4.3$ (Antoniadis et al. 2013). However, as already pointed out by Damour & Esposito-Farèse (1998) a PSR–SBH system would generally be even more asymmetric, since the no-scalar-hair theorem for black holes in scalar–tensor gravity gives (Hawking 1972; Damour & Esposito-Farèse 1992)

$$\alpha_\bullet = 0, \quad \beta_\bullet = 0. \tag{42}$$

Strictly speaking, this is only valid for stationary black holes where the metric is asymptotically flat and the scalar field is asymptotically constant (see Berti et al. 2013 for a detailed discussion on the validity of the classical no-hair theorem and a generalized no-hair theorem in scalar–tensor gravity). However, as we will discuss below, this is still a very good approximation in PSR–SBH systems.

In this section, we will demonstrate that the discovery and timing of a PSR–SBH system in a $P_\mathrm{b} \lesssim 5$ d orbit has the potential to significantly improve existing constraints on scalar–tensor gravity, especially with the next generation of radio telescopes.

4.1 PK parameters in PSR–SBH systems

The parametrized PK formalism can be used not only in GR, but also in a wide class of alternative theories of gravity, including the $T_1(\alpha_0, \beta_0)$ class of scalar–tensor theories discussed here (Damour 1988; Damour & Taylor 1992). The explicit expressions for the PK parameters in $T_1(\alpha_0, \beta_0)$ can be found in Damour & Esposito-Farèse (1996). For a PSR–SBH system equation (42) considerably simplify these expressions. For the quasi-stationary PK parameters one finds

$$\dot{\omega} = \frac{3}{1-e^2}\left(\frac{P_\mathrm{b}}{2\pi}\right)^{-5/3} \frac{G_*^{2/3}}{c^2}\,(M_\mathrm{p}+M_\bullet)^{2/3}, \tag{43}$$

$$\gamma = e\left(\frac{P_\mathrm{b}}{2\pi}\right)^{1/3} \frac{G_*^{2/3}}{c^2}\,\frac{(M_\mathrm{p}+2M_\bullet)M_\bullet}{(M_\mathrm{p}+M_\bullet)^{4/3}}, \tag{44}$$

$$s_\mathrm{Sh} = x\left(\frac{P_\mathrm{b}}{2\pi}\right)^{-2/3} c\,G_*^{-1/3}\,\frac{(M_\mathrm{p}+M_\bullet)^{2/3}}{M_\bullet}, \tag{45}$$

$$r_\mathrm{Sh} = \frac{G_*}{c^3}\,M_\bullet. \tag{46}$$

The bare gravitational constant G_* is related to the gravitational constant measured in a Cavendish experiment by $G = G_*(1+\alpha_0^2)$. Consequently, modulo an unobservable rescaling of the masses,[7] the PK parameters given above are identical to the quasi-stationary PK parameters in GR (cf. equations 3,5,6,8). This agrees with the findings of Mirshekari & Will (2013), that through first post-Newtonian (PN) order (c^{-2}), the motion of a black hole neutron-star system in scalar–tensor gravity is identical to that in GR.

However, the situation is different for the gravitational wave damping (PK parameter $\dot{P}_\mathrm{b}$). Due to the scalar charge of the neutron star, the system would emit gravitational radiation of all multipoles, since the system can now loose energy to scalar waves in addition to energy loss into tensor waves (Damour & Esposito-Farèse 1992; Will 1993). The scalar monopole and quadrupole contributions enter the orbital dynamics at the 2.5 PN level (order c^{-5}), and are normally much smaller than the tensor-quadrupole contribution, given the existing constraints on α_p for pulsars up to $2\,\mathrm{M}_\odot$ (Freire et al. 2012; Antoniadis et al. 2013). Concerning the scalar dipole radiation, the situation is very different, as this contribution affects the orbital dynamics already at the 1.5 PN level (order c^{-3}) and is therefore enhanced (compared to the tensor waves) by a large factor of c^2/v^2, where v is the velocity of the relative motion of the binary. The orbital averaged change in the orbital period up to 2.5 PN order can be written as a sum of scalar ($\varphi^\star$) and tensor (g^*) contributions,

$$\begin{aligned}\dot{P}_\mathrm{b} = {} & \dot{P}_{\mathrm{b},\varphi^*}^{\mathrm{Monopole,2.5PN}} \\ & + \dot{P}_{\mathrm{b},\varphi^*}^{\mathrm{Dipole,1.5PN}} + \dot{P}_{\mathrm{b},\varphi^*}^{\mathrm{Dipole,2.5PN}} \\ & + \dot{P}_{\mathrm{b},\varphi^*}^{\mathrm{Quadrupole,2.5PN}} \\ & + \dot{P}_{\mathrm{b},g^*}^{\mathrm{Quadrupole,2.5PN}},\end{aligned} \tag{47}$$

where for a PSR–BH system ($\alpha_\bullet = \beta_\bullet = 0$) all these terms depend on P_b, e, the (gravitational) masses G_*M_p and $G_*M_\bullet$, and all $\varphi^\star$-terms are proportional to α_p^2 (Damour & Esposito-Farèse 1992). To leading order we have

$$\begin{aligned}\dot{P}_\mathrm{b} = {} & -\frac{192\pi}{5}\left(\frac{P_\mathrm{b}}{2\pi}\right)^{-5/3}\frac{G_*^{5/3}}{c^5}\,\frac{M_\mathrm{p}M_\bullet}{(M_\mathrm{p}+M_\bullet)^{1/3}}\,f(e) \\ & - \frac{4\pi^2}{P_\mathrm{b}}\,\frac{G_*}{c^3}\,\frac{M_\mathrm{p}M_\bullet}{M_\mathrm{p}+M_\bullet}\,\frac{1+e^2/2}{(1-e^2)^{5/2}}\,\alpha_\mathrm{p}^2.\end{aligned} \tag{48}$$

For the still allowed region of $T_1(\alpha_0, \beta_0)$, one can show that the scalar 2.5 PN monopole, dipole and quadrupole terms in equation (47) are several orders of magnitude smaller than the terms in equation (48). The last term (proportional to α_p^2) is the key to constrain scalar–tensor theories with PSR–SBH systems, while the other PK parameters (equations 43–46) merely provide the constraints for the, a priori unknown, masses M_p and $M_\bullet$. For a given EoS, α_p is a function of α_0, β_0 and M_p. Based on this, a measurement or constraint of $\dot{P}_\mathrm{b}$ in a PSR–SBH system, in combination with the measurement of at least two more PK parameters, can be converted into an exclusion area within the α_0–β_0 plane of $T_1(\alpha_0, \beta_0)$ theories.

As discussed in Section 3.2.1, the observed $\dot{\omega}$ can be significantly influenced by the frame dragging caused by the rotation of the black hole. For simplicity, we assume here that the rotation of the black hole is sufficiently small. In practice, if the companion is a fast rotating black hole, one would need a self-consistent analysis, which at the same time provides the spin of the black hole from the Lense–Thirring precession of the orbit. Alternatively, depending on the orientation and eccentricity of the system, the Shapiro delay might give an independent access to M_p and $M_\bullet$.

Finally, the scalar no-hair theorem can be shown to be valid in PSR–SBH systems, based on an order of magnitude estimation. If a pulsar that orbits a black hole in an eccentric orbit carries a scalar charge, it induces a time-variant scalar field at the location of the black hole, given by

$$\varphi_r^{(\mathrm{p})} \approx \varphi_0 + \frac{GM_\mathrm{p}}{c^2 r}\alpha_\mathrm{p}, \tag{49}$$

where r is the relative separation between pulsar and black hole. For an eccentric orbit ($e \neq 0$), r changes on a time-scale of the orbital

[7] It is interesting to point out, that from Cassini we already know that $\alpha_0^2 \lesssim 10^{-5}$. Consequently, a rescaling of the masses by $(1+\alpha_0^2)^{-1}$ is anyhow (generally) small compared to the implicit rescaling due to the unknown systemic radial velocity (Damour & Taylor 1992).

period P_b. According to Jacobson's 'Miracle Hair Growth Formula' (Jacobson 1999; Berti et al. 2013), this induces a scalar charge on a black hole. The corresponding (effective) scalar coupling can be estimated by

$$\alpha_\bullet^{\rm induced} \approx 4\frac{GM_\bullet}{c^3}\,\partial_t\varphi_r^{(\rm p)} \approx 4\frac{GM_\bullet}{c^2 r}\,\frac{GM_{\rm p}}{c^2 r}\,\frac{\dot r}{c}\,\alpha_{\rm p}. \tag{50}$$

For a compact PSR–SBH system ($r \sim 1$ light-second) one finds $GM_\bullet/c^2 r \sim 10^{-5}$, $GM_{\rm p}/c^2 r \sim 10^{-6}$, and $\dot r/c \sim 10^{-3}$. Consequently, the induced scalar coupling is absolutely negligible for the gravity tests outlined in this section.

4.2 Mock data analysis

The potential of a PSR–SBH system in constraining scalar–tensor theories of gravity can be demonstrated by mock data simulations. Here, we assume a PSR–SBH system with $P_b = 5$ d, $e = 0.8$ and $m_p = 1.4$. A stiff EoS allowing a maximum neutron-star mass of $\sim$2.5 $M_\odot$ (Müther, Prakash & Ainsworth 1987) is used to calculate α_p for any given theory $T_1(\alpha_0, \beta_0)$. Note that this choice of EoS leads to conservative constraints, as the application of a softer EoS would generally lead to larger scalar charges for the neutron star and therefore more stringent limits. For the black hole, we have assumed a non-rotating ($\chi = 0$) 10 $M_\odot$ black hole, because a significant spin would only complicate the timing analysis (see Section 3) but should not greatly influence the constraints on scalar–tensor theories. The applied observational scheme is retained as in Section 3.1.2. The simulated TOAs are based on the orbital dynamics of GR, and fitted with the DD timing model to estimate the PK parameters. These measurements are then confronted with equations (43)–(48), in order to exclude those areas of the α_0–β_0 for which no pair (M_p, $M_\bullet$) can be found such that all calculated PK parameters agree with the fitted values within the measurement errors. A more detailed description of tests of $T_1(\alpha_0, \beta_0)$ theories with PK parameters can be found in Damour & Esposito-Farèse (1996).

Fig. 8 presents the results for three different scenarios: 10 yr timing with a 100-m class, 5 yr with the FAST and SKA. The simulations show clearly, that a PSR–SBH system would be a great test-bed for scalar–tensor gravity, in particular with the FAST and the SKA. A few years timing observations of an MSP–SBH system with these future radio telescopes would lead to significantly better constraints, with the potential to greatly exceed Solar system experiments for all values of β_0 (including Jordan–Fierz–Brans–Dicke gravity $\beta_0 = 0$), similar to the expectation from *Gaia*.

As a final remark, for very large β_0 the neutron star nearly completely de-scalarizes, making a PSR–BH system a less sensitive test for scalar–tensor gravity. For instance, for a 1.4 $M_\odot$ neutron star and $\beta_0 = 20$ one finds $\alpha_p \simeq 0.14\,\alpha_0$, and for $\beta_0 = 200$ one gets $\alpha_p \simeq 0.02\,\alpha_0$.

5 EXTERNAL FACTORS

In practice, there are other effects that can contaminate the measured properties used for the GR tests enabled by PSR–SBH systems. The observed secular change of the orbital projected semimajor axis can be influenced by shrinking of the orbit due to gravitational radiation, proper motion of mass centre (Kopeikin 1996), geodetic precession of the pulsar's spin (Damour & Taylor 1992) and a varying Doppler shift caused by secular change in the distance of the binary mass centre and the relative acceleration in the gravitational field of the Galaxy (Shklovskii 1970; Damour & Taylor 1991). Assuming a

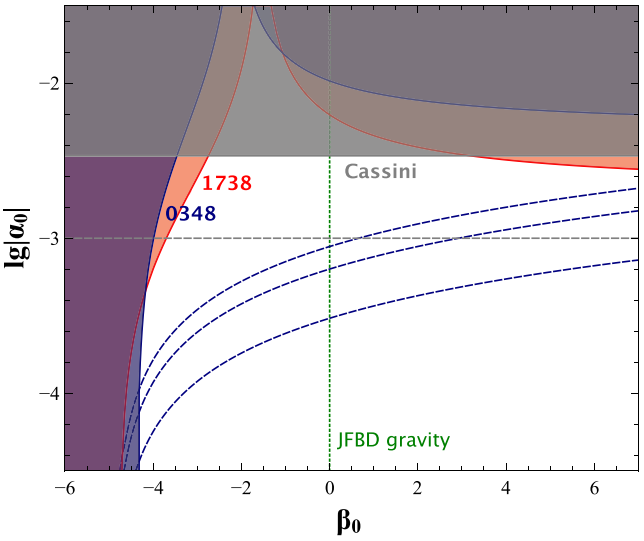

Figure 8. Constraints on $T_1(\alpha_0, \beta_0)$ scalar–tensor theories. Exclusion areas are based on current Solar system and pulsar experiments, taken from Bertotti et al. (2013, 'Cassini'), Freire et al. (2012, '1738') and Antoniadis et al. (2013, '0348'). Blue dashed lines are based on simulations for an MSP–SBH system – from top to bottom: 10 yr with a 100-m class, 5 yr with the FAST and SKA (details can be found in the text). The vertical dashed green line at $\beta_0 = 0$ indicates Jordan–Fierz–Brans–Dicke gravity. The horizontal dashed grey line indicates the limit expected from near future Solar system experiments, foremost the astrometric satellite *Gaia*.

1.4 $M_\odot$ pulsar, one can obtain the comparison of the gravitational wave damping contribution with the spin–orbit effect in GR as (Peters 1964)

$$\left|\frac{\dot x_{\rm gw}}{\dot x_{\rm s}}\right| \simeq 4.8\times10^{-6}\,\frac{f(e)}{|\chi\sin\theta_{\rm S}\sin\Phi\cot i|}\left(\frac{P_b}{1\,\rm d}\right)^{-2/3} m_\bullet^{-1/3}. \tag{51}$$

For a black hole of $m_\bullet = 10$, $\chi = 0.9$, and an orbit of $P_b = 0.1$ d, $e = 0.8$, $\theta_S = \Phi = i = 45^\circ$, the ratio appears to be $\sim 10^{-4}$, suggesting that normally the spin–orbit coupling dominates the secular change of x over gravitational wave damping. The contribution by proper motion of the mass centre could be significant if the binary is close to the Solar system, but in this case can also be measured and subtracted by high-precision astrometry (e.g. Deller et al. 2013) or pulsar timing itself. The contribution by the pulsar's geodetic precession, following Damour & Taylor (1992), can be compared with $\dot x_s$ by

$$\left|\frac{\dot x_{\rm geo}}{\dot x_{\rm s}}\right| \sim 6\times10^{-3}\,\chi^{-1}\left(\frac{P}{1\,\rm s}\right)\left(\frac{P_b}{1\,\rm d}\right)^{-2/3}\left(\frac{m_\bullet}{10}\right)^{-1/3}, \tag{52}$$

where P is the pulsar rotational period. Therefore, the effect is stronger for PSR–BH system with a slow pulsar. With $P = 0.5$ s, $P_b = 0.2$ d, $m_\bullet = 10$ and $\chi = 0.9$, the ratio $\sim 7\times10^{-3}$, indicating that this effect needs to be taken into account only for a slow pulsar in a very compact orbit. The effect of varying Doppler shift contains contributions from relative l.o.s. Galactic acceleration and traverse velocity (the Shklovskii term) between the system and the Solar system barycentre. Its contribution to $\dot x$, as argued in Wex & Kopeikin (1999), will not be important unless the binary system is in the central region of our Galaxy.

The observed secular change of orbital period can also be contaminated by the varying Doppler shift. Recent studies have shown that based on the current Galactic potential model, the contribution

to $\dot{P}_{\rm b}$ caused by the relative l.o.s. acceleration can be corrected at a level of 10^{-15}–10^{-16} (Lazaridis et al. 2009; Freire et al. 2012). The determination of the Shklovskii effect depends on the measurement accuracies of proper motion and distance, and can be expected with high precision from astrometry or pulsar timing itself (e.g. Smits et al. 2011; Deller et al. 2013). In this case, the precision of the Galactic potential model is more likely to be a limiting factor for dipole radiation tests. The varying Doppler shift may also limit the precision of mass determination with $\dot{P}_{\rm b}$ and thus the cosmic censorship conjecture test, especially for wide orbits with small $\dot{P}_{\rm b}$ ($\lesssim 10^{-14}$). Nevertheless, one might be able to use the measurement of the Shapiro delay instead to determine the masses, which in this case would be anyway determined with better precision for systems of sufficiently edge-on geometry (i.e., $i \gtrsim 60^{\circ}$).

The geodetic precession of the pulsar spin will result variation in pulse profiles (e.g. Kramer 1998), which may complicate or limit the pulsar-timing precision. For the worst case, it might even turn the radiation beam away from our l.o.s. (Perera et al. 2010). To leading order the spin precession is given by the geodetic precession rate, which for $m_{\bullet} \gg m_{\rm p}$ reads (Barker & O'Connell 1975)

$$\Omega_{\rm geod} \approx (0.5\,{\rm deg\,yr^{-1}}) \frac{1}{1-e^2} \left(\frac{P_{\rm b}}{1\,{\rm d}}\right)^{-5/3} \left(\frac{m_{\bullet}}{10}\right)^{2/3}. \quad (53)$$

Consequently, for an orbit of $P_{\rm b} = 0.1$ d, $m_{\bullet} = 10$ and $e = 0.1$ the precession rate is roughly 22 deg yr^{-1}. Fortunately, the spin geometry of the pulsar can also be studied from polarimetric information (e.g. Kramer 1998; Manchester et al. 2010), which may provide a method to properly model the profile evolution and still enable high-precision timing. On the other hand, the observation of the geodetic precession can give access to a further PK parameter, if the precession rate can be determined independently. Unfortunately, even if an independent measurement of the precession rate is possible, it is not expected to give a high-precision value, like for the other PK parameters (cf. Breton et al. 2008; Fonseca, Stairs & Thorsett 2014 for two binary pulsar systems, where the geodetic precession rate has been measured). Still, there could be important information coming from modelling the geodetic precession of the pulsar. In general, the spin of the SBH companion is much larger than that of the pulsar. But in the case of a fast rotating pulsar (MSP) and a slowly rotating ($\chi \lesssim 0.1$) low-mass ($m_{\bullet} \lesssim 5$) SBH, the pulsar spin can easily reach ~10 per cent of the SBH spin, giving a corresponding contribution to the relativistic spin–orbit coupling. In such a case the orientation of the pulsar spin, coming from the observation of the geodetic precession, is needed to extract the SBH spin from the observed Lense–Thirring precession of the orbit.

6 SEARCHES FOR PULSAR–BLACK HOLE BINARIES

Searches for undiscovered pulsars have been extensively performed ever since the first discovery in 1967 (Hewish et al. 1968). Despite improvements in both observational hardware and data processing techniques, the discovery of a PSR–SBH system has so far eluded pulsar astronomers. Although it is expected that PSR–SBH systems are rare, it can be shown that observational selection effects could have played an important role in the non-detection. Pulsars in binary systems show periodic changes in their spin frequency because of Doppler effects induced by orbital motion. In compact, high-mass, or eccentric systems these effects can manifest themselves within the time-scale of individual pulsar survey observations i.e. typically of the order of minutes. Standard Fourier based searches, that look for significant features in the power spectrum of dedispersed time series, are not sensitive to pulsar spin frequencies that change, since power is smeared over a number of spectral bins, reducing the detection signal-to-noise (S/N) ratio (see e.g. Johnston & Kulkarni 1991; Ransom, Eikenberry & Middleditch 2002). To combat the detrimental effects of orbital motion, pulsar searches typically employ computationally intensive binary search algorithms, such as 'acceleration searches' (for a summary of current methods, see Lorimer & Kramer 2005). Like in pulsar 'drift scan' surveys (e.g. Deneva et al. 2013), many of these effects can be overcome by reducing the dwell time of survey observations; a possibility offered by the supreme instantaneous sensitivity of next generation telescopes. In this section, we investigate the basic search requirements for the detection of PSR–SBH systems.

6.1 Acceleration searches and computational considerations

Changes in the apparent spin frequency are caused by the varying l.o.s. velocity of the pulsar, $v(t)$, as it orbits its companion. The apparent spin frequency as a function of time, $\nu_{\rm app}(t)$, is given by the Doppler formula

$$\nu_{\rm app}(t) = \nu \left(1 - \frac{v(t)}{c}\right), \quad (54)$$

where $v(t)$ can be described by five Keplerian orbital parameters. If these parameters are known, it is possible to resample the time series and transform it into a frame inertial with respect to the pulsar. Standard Fourier methods can then be used to detect the periodic signal from a pulsar with no reduction in S/N. However, in a blind search, where the orbital parameters are initially unknown, a five-dimensional search is computationally prohibitive (see e.g. Knispel et al. 2013). If the observing time ($T_{\rm obs}$) is a small fraction of the orbital period, the l.o.s. velocity can be approximated in a Taylor expansion:

$$v(t) \approx v_0 + a_0 t + j_0 t^2/2 + ..., \quad (55)$$

where v_0, a_0 and j_0 are the average values of velocity, acceleration and rate of change of acceleration – 'jerk', respectively. When $T_{\rm obs}$ is sufficiently small (see e.g. $T_{\rm obs} \lesssim P_{\rm b}/10$ from Ransom, Cordes & Eikenberry 2003, Ng et al. in preparation), time or equivalent frequency domain searches in only constant acceleration, given by the first-order term, $v(t) \simeq a_0 t$ (the constant v_0 can be dropped here), are effective (e.g. Camilo et al. 2000; Ransom et al. 2002; Eatough et al. 2013).

For the detection of binary systems where large changes in acceleration are observed (see Section 6.2), improvements in S/N are offered by searches in higher order velocity derivatives (see e.g. Bagchi, Lorimer & Wolfe 2013; Eatough et al. 2013; Knispel et al. 2013), at the cost of at least an order of magnitude more computational operations. It is expected that pulsar searches to be performed with the SKA will be performed in real time or 'pseudo-real-time',[8] to cope with data output volumes. Because first-order acceleration searches already constitute a significant data processing task[9] higher order realtime searches are unlikely to be performed, unless adequate computational hardware or software

[8] To achieve the specified limiting sensitivity to periodic pulsed signals, the full integration time will be completed before data processing can commence.

[9] In table 24 of Dewdney et al. (2013), it is shown that the data processing for a pulsar survey with SKA1-mid is dominated by the acceleration search processing load of nearly 10 peta operations per second; 10 times the

becomes available.[10] With reference to the latter, we notice that significant progress in speeding up various aspects of pulsar search code has been made in recent years, primarily through the use of GPU technology[11,12] (see e.g. Barsdell, Barnes & Fluke 2010; Magro et al. 2011; Armour et al. 2012; Barsdell et al. 2012; Barr et al. in preparation). In the following sections, our investigation is limited to searches utilizing the constant acceleration approximation only.

6.1.1 PSR–SBH orbital acceleration characteristics

It is useful to consider the degree of orbital acceleration that might be observable in compact or eccentric PSR–SBH systems as this gives the parameter space that needs to be searched with acceleration searches, and rough estimates of the corresponding level of computation required (Section 6.1.2). In Fig. 9, panels (a), (b) and (c), the expected value of l.o.s. acceleration as a function of observation time is given for various extreme PSR–SBH systems. Panel (a) shows the results for compact ($P_b = 2.4$ h) near circular systems ($e = 0.1$) and panels (b) and (c) show longer orbital period ($P_b = 12.0$ h) eccentric ($e = 0.8$) systems. In both cases, the binary systems are viewed edge-on ($i = 90^\circ$), where the effects of l.o.s. motion are strongest, and thick lines (both solid and dashed) show the acceleration for systems with $\omega = 0^\circ$ and thin solid and dashed lines show systems which have the major axis of the pulsar orbit pointed towards the l.o.s. ($\omega = 90^\circ$). L.o.s. pulsar acceleration values have been plotted for two companion black hole masses of 10 and 30 $M_\odot$, and in panel (a) values for a neutron-star companion of 1.3 $M_\odot$ have also been plotted. The l.o.s. pulsar acceleration values have all been calculated using equation (4) in Freire, Kramer & Lyne (2001, 2009) which is derived from Kepler's laws.

From Fig. 9, we would like to draw the readers' attention to two points. First, and as expected, the maximum accelerations that might be observable in PSR–SBH systems can greatly exceed those seen in currently known highly relativistic binary systems. This can be seen by comparison of the acceleration values plotted for the 1.3 $M_\odot$ companion and the black hole companions in panel (a). Here, the double neutron star system (DNS) orbital parameters closely resemble the most relativistic binary pulsar system currently known, the Double Pulsar, PSRs J0737−3039A/B, where the l.o.s. acceleration tops out at $\sim$260 m s^{-2}. While compact PSR–SBH systems of the same orbital period have maximum acceleration values well above this ($\gtrsim$600 m s^{-2}), the most extreme example is shown in the eccentric system where with the appropriate orientation of the major axis of the orbit to the l.o.s. the acceleration can reach nearly 3000 m s^{-2} (see Fig. 9, panel c).

Secondly, in compact PSR–SBH systems (panel a) the acceleration derivatives (jerk) are significantly increased in comparison to DNS of the same orbital period. Considering the first 0.25 h of the orbits in the systems with $\omega = 0$, we find $|j| \sim 0.2$, 0.6 and 0.9 m s^{-3} for companion masses of 1.3, 10 and 30 $M_\odot$, respectively. As we will show in Section 6.2, despite acceleration searches performed on time series that have a length where $T_{obs} \lesssim P_b/10$, these higher order effects can still degrade the effectiveness of the acceleration search method. It is also worth noting that pulsars in eccentric systems, like those displayed in panels (b) and (c), spend the majority

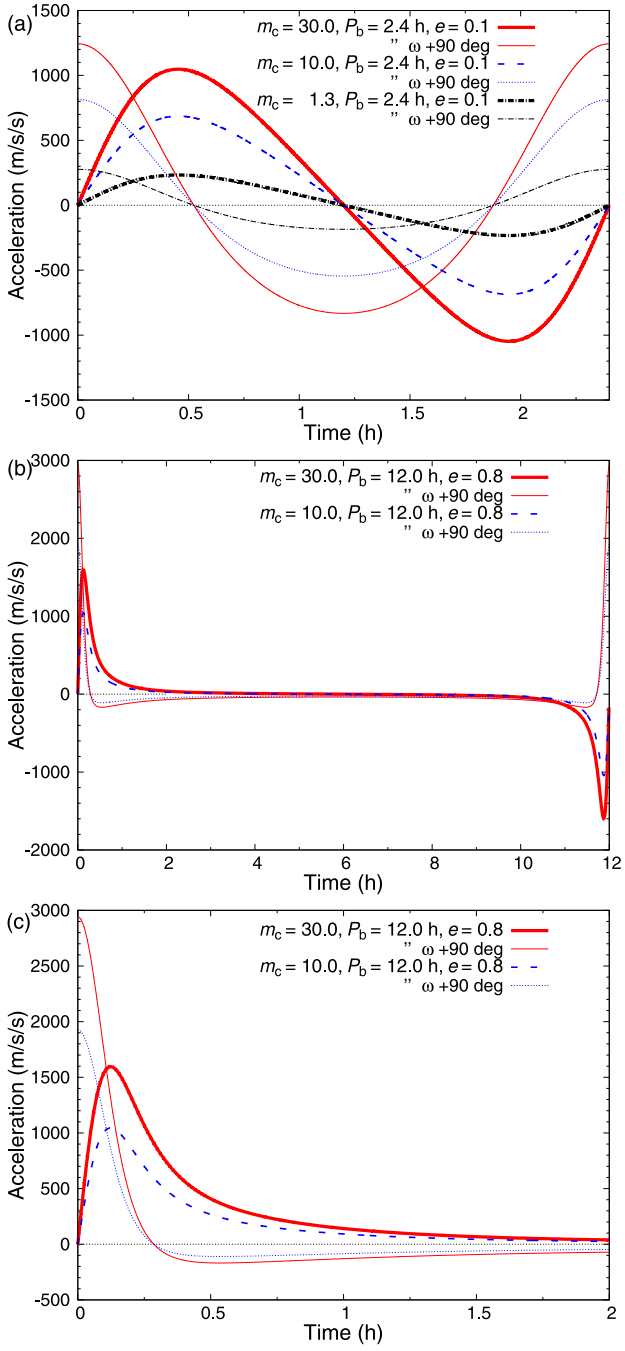

Figure 9. The expected l.o.s. acceleration as a function of time in speculative relativistic binary pulsar systems. Panel (a) shows compact, $P_b = 2.4$ h, near circular, $e = 0.1$, systems while panel (b) shows longer orbital period, $P_b = 12.0$ h, eccentric, $e = 0.8$, systems. Panel (c) shows a zoom-in of the first 2 h of the latter. In both cases black hole masses of 10 and 30 $M_\odot$, and extremes in longitude of periastron, ω have been plotted. In panel (a), the expected values for a compact DNS system (pulsar companion mass of 1.3 $M_\odot$) have also been included. In all cases, the systems are viewed edge-on i.e. $i = 90^\circ$.

processing power offered by the Einstein@Home network as of January 2013: http://einstein.phys.uwm.edu/.

[10] Following the SKA1-mid survey parameters outlined in table 24 of Dewdney et al. (2013), and correcting for a jerk of ± 0.2 m s^{-3} (a value that could be observed in known compact double neutron star systems: see Section 6.1.1), we find that a pseudo-real-time acceleration and jerk search would require over an exaflop per second of computation. By covering the increased acceleration and jerk parameter ranges expected to be observed in PSR–SBH (Section 6.1.1), the computational cost could be higher.

[11] https://github.com/jintaoluo/presto_on_gpu

[12] https://github.com/ewanbarr/peasoup

of the time in a state of low and constant orbital acceleration. However, at periastron the acceleration and jerk can reach values that might not be possible to correct for in real time processing due to computational restrictions (see Section 6.1.2).

6.1.2 *Computational scaling*

The dominant fraction of computing time in pulsar search processing is typically spent at the acceleration search stage, where the entire search process is essentially repeated a large number of times for a number of trial accelerations. As such, consideration of the level of computation required to find PSR–SBH with next generation telescopes is needed to test the feasibility. Here, we limit our discussion to time-domain acceleration searches where the approximate number of computational operations for acceleration searches, $C_{\rm a}$, is proportional to the product of number of trial accelerations, $n_{\rm a}$, and the standard Fast Fourier Transformation (FFT) operation count for one-dimensional real valued data,

$$C_{\rm a} \propto n_{\rm a}\, 2.5\, n_{\rm samp}\, \log_2(n_{\rm samp}), \tag{56}$$

where $n_{\rm a} = \Delta a/\delta a$ and $n_{\rm samp} = T_{\rm obs}/\tau_{\rm samp}$; here, Δa is the total range of trial accelerations searched, δa is the step-size in acceleration over this range and $\tau_{\rm samp}$ is data sampling interval. Estimating the exact number of computational operations in an acceleration search is difficult since a pulsar search consists of not just simple processes like FFTs, but many other operations, such as spectral normalization, harmonic summation, spectral interpolation and the memory access and any associated input/output operations (for details of pulsar search processes, see Lorimer & Kramer 2005). Estimating the computational run time is even more problematic and strongly depends on the hardware being used. Representative tests typically only come from code benchmarking. However, in the following we can derive the relevant computational operation scaling for time-domain acceleration searches; additional overheads would scale in a similar manner.

Following Camilo et al. (2000) and choosing a step-size in acceleration given by $\delta a = Pc/T_{\rm obs}^2$ (P is the pulsar spin period), we can write

$$C_{\rm a} \propto 2.5\, \frac{\Delta a\, T_{\rm obs}^3}{P\, c\, \tau_{\rm samp}}\, \log_2\left(\frac{T_{\rm obs}}{\tau_{\rm samp}}\right). \tag{57}$$

Typically, P is set to the minimum spin period pulsar likely to be detected (e.g. ~ 1 ms); however, to perform an optimal search, one should consider not just the fundamental spin period but the highest spin frequency harmonic that might be detected, e.g. at $P/8$. The best solution is to consider the highest spin frequency that can be detected, which is given by the Nyquist frequency, $f_{\rm Nyq} = 1/2\tau_{\rm samp}$, giving a minimum spin period of $2\tau_{\rm samp}$. Substitution for P in equation (57) gives

$$C_{\rm a} \propto 1.25\, \frac{\Delta a\, T_{\rm obs}^3}{c\, \tau_{\rm samp}^2}\, \log_2\left(\frac{T_{\rm obs}}{\tau_{\rm samp}}\right). \tag{58}$$

These relations are useful for considering the computational cost of acceleration searches, and are of particular importance for realtime searches. For instance, it can be clearly seen that the integration time has the biggest impact on the level of computation required ($C_{\rm a} \propto T_{\rm obs}^3$); an important reason to keep $T_{\rm obs}$ as short as possible. In searches for PSR–SBH, Δa should encompass the maximum l.o.s. accelerations that might be observable in these systems, like those displayed in Fig. 9: $\Delta a \approx \pm 1000\,{\rm m\,s^{-2}}$. Δa can in principle be reduced by a factor $\sin(i)$, where i is the orbital inclination with respect to the observer. For example, a median inclination of 60° could be assumed; however, ensuring that acceleration searches can recover the signal from PSR–SBH systems viewed edge-on is the 'safest' option. Other reductions in the level of computation required can be achieved by assuming larger values for P or accounting for the increasing values of $\tau_{\rm samp}$ typically implemented when large dispersion measure (DM) trials are executed.

From equation (57) and following the SKA1-mid survey parameters outlined in table 24 of Dewdney et al. (2013), it can be shown that an acceleration search for PSR–SBH systems, like those displayed in Fig. 9 (i.e. where $\Delta a \approx \pm 1000\,{\rm m\,s^{-2}}$), would require at least an order of magnitude more computational capacity than currently planned. An approximately equivalent level of computation can be achieved either by adjusting the acceleration step-size to assume a minimum spin period of 20 ms (cf. 2 ms in Dewdney et al. 2013), increasing the sampling interval by a factor of 9, or by reducing the survey integration time from 600 to 278 s. Alternative derivations of acceleration step-sizes can also lead to reduced levels of computation (see e.g. Eatough et al. 2013); however, tests have shown that step-sizes which account for the highest detectable spin frequency harmonic (as described above) have better performance.

We also note that equivalent frequency domain acceleration searches have the potential to probe the large values of acceleration that might be observable in PSR–SBH, or indeed much higher values, for the same or less computational cost (Ransom et al. 2002). Frequency domain methods offer this prospect because the acceleration values searched by such algorithms are proportional to the spin period: $a = n_{\rm drift} cP/T_{\rm obs}^2$, here a is the acceleration and $n_{\rm drift}$ is the number of spectral bins drifted by the signal (see e.g. Hessels 2007). For example, for a spin period of 0.5 s and an observation time of 600 s, a spectral bin drift of $n_{\rm drift} \sim 2.4$ corresponds to an acceleration of $1000\,{\rm m\,s^{-2}}$. Such values of $n_{\rm drift}$ are readily probed with current computational hardware and software[13] (see e.g. Lynch et al. 2011).

Initial surveys to be performed with FAST will include drift scan surveys at lower frequencies (400 MHz; Yue, Li & Nan 2013). Because of the extremely short integration time (~40 s), these surveys will be sensitive to potential nearby PSR–SBH systems. Such short integration lengths will also enable advanced binary searches including jerk, or orbital parameters, to be done.

6.2 Searches of simulated PSR–SBH

We can investigate the effectiveness of acceleration searches in recovering the pulsar signal in PSR–SBH. Establishing the sensitivity of a pulsar acceleration search algorithm is a difficult task since a number of parameters of both the binary system and the observing system can affect the performance; examples include the orbital period, orbital phase at which the observation was performed, eccentricity of the orbit, companion mass, spin period and observation length. To address this issue Bagchi et al. (2013) have extended the work of Johnston & Kulkarni (1991) to analytically define the expected signal loss after acceleration searches or acceleration and jerk searches for binary pulsar systems and observing systems of arbitrary type. Here, we have investigated the effectiveness of acceleration search methods through simulations of the example PSR–SBH systems described in Section 6.1.1.

In Fig. 10, we plot the acceleration value and percentage of spectral power that can be recovered in constant acceleration searches

[13] http://www.cv.nrao.edu/~sransom/presto/

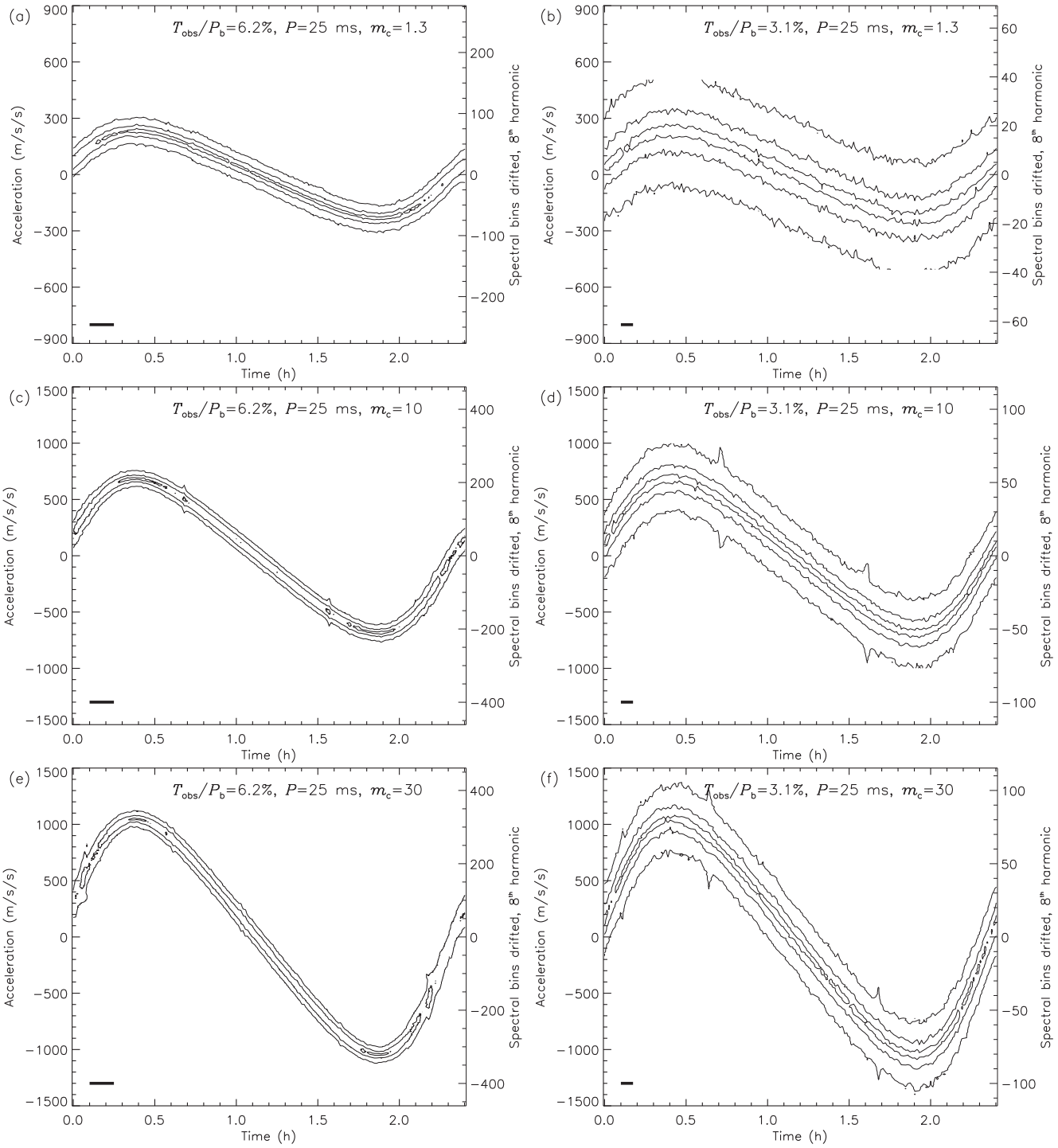

Figure 10. Contours of the recovered spectral power achieved in acceleration searches, incremented in orbital phase, of simulated binary pulsar systems with orbital periods of $P_b = 2.4$ h, $e = 0.1$ and pulsar spin periods of 25 ms. Results are plotted for pulsar companion masses of 1.3 $M_\odot$ (panels a and b – DNS), 10 $M_\odot$ (panels c and d – PSR–SBH) and 30 $M_\odot$ (panels e and f – PSR–SBH), and integration times that cover 6.2 and 3.1 per cent of the 2.4 h orbital period (panels a, c, e and panels b, d, f, respectively). Contours mark 30, 60 and 90 per cent recovery levels of the pulsar signal from an acceleration search. The thick horizontal black bars indicate the length of integration used in the acceleration analysis. The starting point of each acceleration search was incremented in orbital phase by 50 s. In panel (b), 30 per cent recovery contours at extrema in acceleration are not visible due to the finite range of accelerations searched ($\pm 506\,\mathrm{m\,s^{-2}}$).

performed at various orbital phases, and with two representative integration times. Contours mark the 30, 60 and 90 per cent recovery levels, where the percentage is that of the spectral power collected in a search of an equivalent unaccelerated solitary pulsar.

Here we consider compact systems of low eccentricity ($e = 0.1$), where there is more chance the pulsar has undergone a period of recycling. A spin period of 25 ms and a four per cent pulse width have been applied. In all cases, the starting point of the

acceleration searches are incremented in time across the orbit by 50 s and an acceleration step-size, δa, that accounts for the eighth pulsar harmonic has been chosen. On the right-hand y-axis, we give the number of spectral bins drifted ($n_{\rm drift}$) by this eighth harmonic of the spin frequency: a number relevant to acceleration searches performed in the frequency domain (Ransom et al. 2002). Both the simulation of data and the search are conducted with an updated version of the SIGPROC software package.[14] Panel (a) shows that for an observing time of 6.2 per cent of the orbital period (≈537 s) the search succeeds in recovering over 90 per cent of the power at most orbital phases when the companion is of solar mass. However, for PSR–SBH systems observed with this integration time (panels c and e) the same level of recovery can only be achieved at orbital phases where the variation of acceleration is minimized, i.e. at the peaks and troughs. When the observing time is halved to ≈268 s, 90 per cent signal recovery is achievable for observations starting at most orbital phases and for companion masses up to 30 $M_\odot$. Importantly, in terms of limiting telescope sensitivity, the 60 per cent contours in the longer 537 s integrations, displayed in panels (a), (c) and (e), are roughly equivalent to the 90 per cent contours in the shorter 268 s integrations (panels b, d and f). Direct comparison of these contours shows that sensitivity across the orbit is marginally worse in the longer integrations, however, over eight times more computations are required to reach this identical sensitivity level.

In Fig. 11, the results of acceleration searches of a simulated PSR–SBH system ($m_\bullet = 30$) with a wide ($P_{\rm b} = 12.0$ h) and eccentric ($e = 0.8$) orbit is given. Both slow pulsars ($P = 0.5$ s) and recycled ($P = 25$ ms) have been investigated. Fig. 11, panel (a) where $T_{\rm obs} \approx 268$ s, shows the recycled pulsar can be detected with almost full sensitivity at relatively low accelerations ($|a| \lesssim 100$ m s^{-2}) throughout the majority ($\gtrsim 90$ per cent) of the orbit. However, close to periastron, as displayed in panel (b), acceleration searches, even of this reduced integration time that works well in the low-eccentricity systems (Fig. 10, panel f), are not short enough to recover the pulsar signal. This indicates higher order corrections are necessary for detection near periastron. For a longer spin period pulsar ($P = 0.5$ s) in the same system, displayed in panel (c), 90 per cent signal recovery is achieved for observations starting much closer to periastron, even with longer integration times ($T_{\rm obs} \approx 537$ s).

These simulations have demonstrated that within the scope of constant acceleration searches for PSR–SBH, it is important to keep a comparatively short observing time. Our results suggest that integration times of the order 500 s (e.g. Smits et al. 2009; Dewdney et al. 2013) to be performed with the SKA and SKA1 might be too long to guarantee full instrumental sensitivity to the extreme PSR–SBH systems described here; unless the pulsar has a longer spin period (e.g. 0.5 s). Based on probability arguments, high-eccentricity PSR–SBH, containing pulsars of any spin period, are easier to detect as the pulsar spends the majority of time with low and constant l.o.s. acceleration; such systems would also not be strongly selected against with longer integrations. Nevertheless, our simulations indicate that integration times of the order of ∼300 s seem to be the maximum length with which most possible PSR–SBH systems can be detected using constant acceleration search algorithms.

The great improvement in instrumental gain by the next generation of radio telescopes would easily compensate for the loss of sensitivity caused by shortening the integration time. For instance, the currently ongoing deep Galactic plane section of the High Time Resolution Universe Pulsar Survey (HTRU-Deep) has an integration time of 4300 s with the Parkes Radio Telescope (e.g. Keith et al. 2010; Ng et al. in preparation). Assuming a telescope gain of ∼100 K Jy^{-1}, an SKA survey with 300 s integration time would still enable a factor of 20–30 increase in sensitivity. Following the

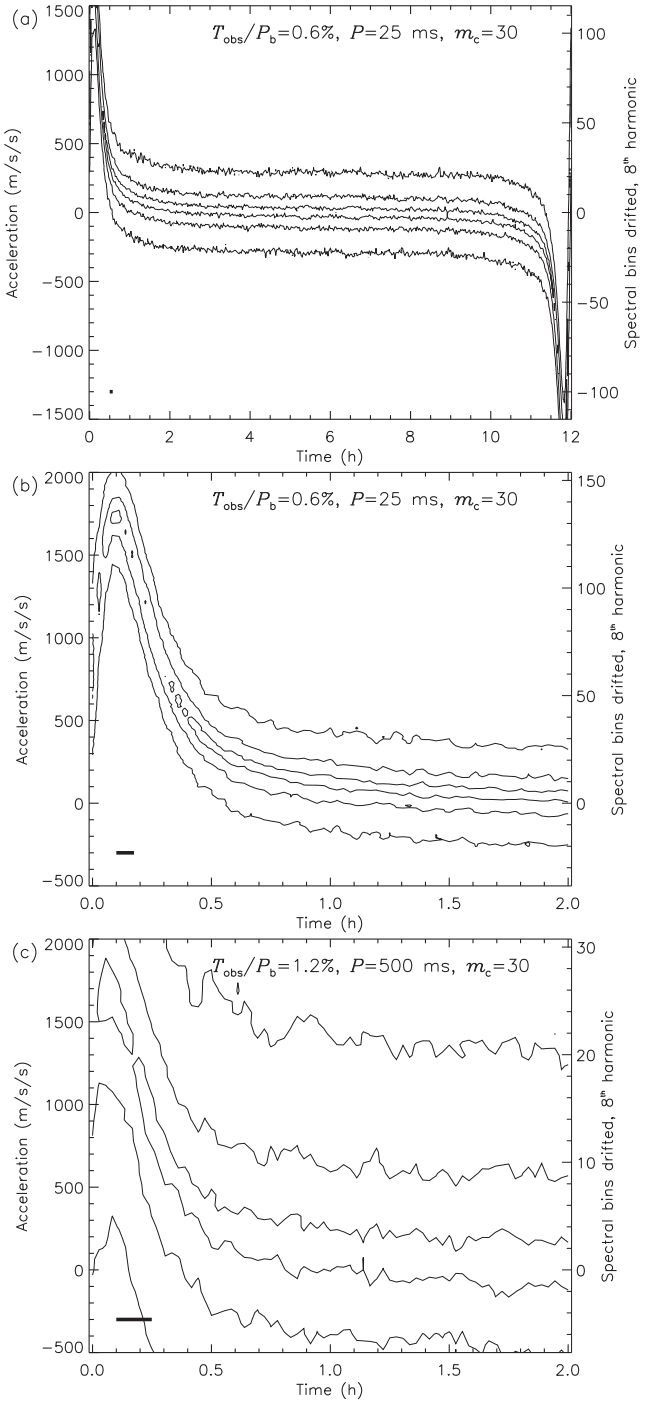

Figure 11. Contours of the recovered spectral power achieved in acceleration searches, incremented in orbital phase (by 100 s), of a simulated PSR–SBH system with an orbital period of $P_{\rm b} = 12.0$ h and $e = 0.8$. Panels (b) and (c) show a zoom-in of the first 0.25 h of the full orbit displayed in panel (a). In panel (c), the pulsar spin period is increased from 25 ms (panels a and b) to 0.5 s. The representation of lines is the same as in Fig. 10.

[14] http://sigproc.sourceforge.net/

above comparison to HTRU-Deep we find a factor of 2 improvement in sensitivity with a FAST drift scan survey.

7 CONCLUSIONS

In this paper, we investigate the achievable gravity tests by observing a PSR–SBH binary system, in particular with the next generation of radio telescopes. For our studies, we have used the sensitivity of the FAST and SKA as representatives for the future telescopes. The investigations are based on simulated pulsar-timing data with consistent timing models. It has been shown that with 3–5 yr pulsar-timing observations, we can expect to measure the masses of the pulsar and the black hole with high precision (e.g. 0.001–1 per cent), especially when the pulsar is an MSP and the observations are conducted with the next generation of radio telescopes. The black hole spin can be measurable on time-scales of 5–10 yr, with high precision ($\sim$1 per cent) on the same optimal scenario. Those measurements will lead to a test of GR's cosmic censorship conjecture. The quadrupole of the black hole is measurable only when the pulsar is fully recycled and the system is of extreme configuration, in terms of orbit compactness or mass of the black hole. In addition, we showed that a PSR–SBH system would enable a few orders of magnitude improvement in constraining alternative gravity theories which predicts practically identical black holes to GR. This is demonstrated with the help of a specific class of scalar–tensor theories of gravity.

Finally, we have investigated some of the requirements in searches for PSR–SBH. The large instantaneous sensitivity of next generation of radio telescopes should allow reduced pulsar survey integration times, thereby enabling the potentially extreme orbital parameter space associated with PSR–SBH to be searched more effectively.

ACKNOWLEDGEMENTS

We thank P. C. C. Freire and S. M. Ransom for useful discussions and reading the manuscript. We are grateful to J. Lattimer for providing the tables for equations-of-state MPA1. We also wish to thank the anonymous referee for valuable comments. KL is supported by the ERC Advanced Grant 'LEAP', Grant Agreement Number 227947 (PI: MK).

REFERENCES

Antoniadis J. et al., 2013, Science, 340, 448
Armour W. et al., 2012, in Ballester P., Egret D., Lorente N. P. F., eds, ASP Conf. Ser. Vol. 461, Astronomical Data Analysis Software and Systems XXI. Astron. Soc. Pac., San Francisco, p. 33
Bagchi M., Lorimer D. R., Wolfe S., 2013, MNRAS, 432, 1303
Barker B. M., O'Connell R. F., 1975, Phys. Rev. D, 12, 329
Barsdell B. R., Barnes D. G., Fluke C. J., 2010, MNRAS, 408, 1936
Barsdell B. R., Bailes M., Barnes D. G., Fluke C. J., 2012, MNRAS, 422, 379
Belczynski K., Bulik T., Fryer C. L., Ruiter A., Valsecchi F., Vink J. S., Hurley J. R., 2010, ApJ, 714, 1217
Berti E., Cardoso V., Gualtieri L., Horbatsch M., Sperhake U., 2013, Phys. Rev. D, 87, 124020
Bertotti B., Iess L., Tortora P., 2003, Nature, 425, 374
Blandford R., Teukolsky S. A., 1976, ApJ, 205, 580
Breton R. P. et al., 2008, Science, 321, 104
Camilo F., Lorimer D. R., Freire P., Lyne A. G., Manchester R. N., 2000, ApJ, 535, 975
Clausen D., Sigurdsson S., Chernoff D. F., 2014, MNRAS, 442, 207
Cordes J. M., Shannon R. M., 2010, preprint (arXiv:1107.3086)
Damour T., 1988, in Coley A., Dyer C., Tupper T., eds, Proc. 2nd Canadian Conf. on General Relativity and Relativistic Astrophysics. World Scientific Press, Singapore, p. 315
Damour T., 2009, in Colpi M., Casella P., Gorini V., Moschella U., Possenti A., eds, Astrophys. Space Sci. Libr., Vol. 359, p. 1
Damour T., Deruelle N., 1986, Ann. Inst. Henri Poincaré Phys. Theor., 44, 263
Damour T., Esposito-Farèse G., 1992, Class. Quant Gravity, 9, 2093
Damour T., Esposito-Farèse G., 1993, Phys. Rev. Lett., 70, 2220
Damour T., Esposito-Farèse G., 1996, Phys. Rev. D, 54, 1474
Damour T., Esposito-Farèse G., 1998, Phys. Rev. D, 58, 1
Damour T., Taylor J. H., 1991, ApJ, 366, 501
Damour T., Taylor J. H., 1992, Phys. Rev. D, 45, 1840
Deller A. T., Boyles J., Lorimer D. R., Kaspi V. M., McLaughlin M. A., Ransom S., Stairs I. H., Stovall K., 2013, ApJ, 770, 145
Deneva J. S., Stovall K., McLaughlin M. A., Bates S. D., Freire P. C. C., Martinez J. G., Jenet F., Bagchi M., 2013, ApJ, 775, 51
Dewdney P. E., Turner W., Millenaar McCool R., Lazio J., Cornwell T. J., 2013, SKA1 System Baseline Design (SKA-TEL-SKO-DD-001), https://www.skatelescope.org/wp-content/uploads/2013/05/SKA-TEL-SKO-DD-001-1_BaselineDesign1.pdf
Eatough R. P., 2009, PhD thesis, Univ. Manchester
Eatough R. P., Kramer M., Lyne A. G., Keith M. J., 2013, MNRAS, 431, 292
Esposito-Farèse G., 2009, preprint (arXiv:0905.2575)
Faucher-Giguère C.-A., Loeb A., 2011, MNRAS, 415, 3951
Fonseca E., Stairs I. H., Thorsett S. E., 2014, ApJ, 787, 82
Freire P. C., Kramer M., Lyne A. G., 2001, MNRAS, 322, 885
Freire P. C., Gupta Y., Ransom S. M., Ishwara-Chandra C. H., 2004, ApJ, 606, L53
Freire P. C. C., Ransom S. M., Gupta Y., 2007, ApJ, 662, 1177
Freire P. C., Kramer M., Lyne A. G., 2009, MNRAS, 395, 1775
Freire P. C. C. et al., 2012, MNRAS, 423, 3328
Garfinkel B., 1958, AJ, 63, 88
Garfinkel B., 1959, AJ, 64, 353
Gou L. et al., 2011, ApJ, 742, 85
Gou L. et al., 2014, ApJ, 790, 29
Hansen R. O., 1974, J. Math. Phys., 15, 46
Hawking S. W., 1972, Commun. Math. Phys., 25, 167
Hessels J. W. T., 2007, PhD thesis, McGill Univ., Canada
Hewish A., Bell S. J., Pilkington J. D. H., Scott P. F., Collins R. A., 1968, Nature, 217, 709
Hulse R. A., Taylor J. H., 1975, ApJ, 195, L51
Jacobson T., 1999, Phys. Rev. Lett., 83, 2699
Jenet F. A., Gil J., 2004, ApJ, 602, L89
Jenet F., Anderson S., Kaspi V., Prince T., Unwin S., 1998, ApJ, 498, 365
Johnston H. M., Kulkarni S. R., 1991, ApJ, 368, 504
Keith M. J. et al., 2010, MNRAS, 409, 619
Knispel B. et al., 2010, Science, 329, 1305
Knispel B. et al., 2013, ApJ, 774, 93
Kopeikin S. M., 1996, ApJ, 467, L93
Kramer M., 1998, ApJ, 509, 856
Kramer M., Backer D. C., Cordes J. M., Lazio T. J. W., Stappers B. W., Johnston S., 2004, New Astron. Rev., 48, 993
Lazaridis K. et al., 2009, MNRAS, 400, 805
Lazio T. J. W., 2013, Class. Quantum Gravity, 30, 224011
Lense J., Thirring H., 1918, Phys. Z., 19, 156
Liu K., 2012, PhD thesis, Univ. Manchester
Liu K., Verbiest J. P. W., Kramer M., Stappers B. W., van Straten W., Cordes J. M., 2011, MNRAS, 417, 2916
Liu K., Wex N., Kramer M., Cordes J. M., Lazio T. J. W., 2012, ApJ, 747, 1
Lorimer D. R., Kramer M., 2005, Handbook of Pulsar Astronomy. Cambridge Univ. Press, Cambridge
Lynch R. S., Ransom S. M., Freire P. C. C., Stairs I. H., 2011, ApJ, 734, 89
Lynch R. S., Freire P. C. C., Ransom S. M., Jacoby B. A., 2012, ApJ, 745, 109

Lyne A., Hobbs G., Kramer M., Stairs I., Stappers B., 2010, Science, 329, 408
Magro A., Karastergiou A., Salvini S., Mort B., Dulwich F., Zarb Adami K., 2011, MNRAS, 417, 2642
Manchester R. N. et al., 2010, ApJ, 710, 1694
Mirshekari S., Will C. M., 2013, Phys. Rev. D, 87, 084070
Müther H., Prakash M., Ainsworth T. L., 1987, Phys. Lett. B, 199, 469
Nan R., 2006, Sci. China G, 49, 129
Nan R. et al., 2011, Int. J. Mod. Phys. D, 20, 989
Narayan R., McClintock J. E., 2013, preprint (arXiv:1312.6698)
Osłowski S., van Straten W., Hobbs G. B., Bailes M., Demorest P., 2011, MNRAS, 418, 1258
Penrose R., 1979, in Hawking S. W., Israel W., eds, General Relativity: An Einstein Centenary Survey, Vol. 1. Cambridge Univ. Press, Cambridge, p. 581
Perera B. B. P. et al., 2010, ApJ, 721, 1193
Peters P. C., 1964, Phys. Rev., 136, 1224
Pfahl E., Podsiadlowski P., Rappaport S., 2005, ApJ, 628, 343
Price R. H., 1972a, Phys. Rev. D, 5, 2419
Price R. H., 1972b, Phys. Rev. D, 5, 2439
Prince T. A., Anderson S. B., Kulkarni S. R., Wolszczan W., 1991, ApJ, 374, L41
Ransom S. M., Eikenberry S. S., Middleditch J., 2002, AJ, 124, 1788
Ransom S. M., Cordes J. M., Eikenberry S. S., 2003, ApJ, 589, 911
Robertson H. P., 1938, Ann. Math., 39, 101
Ryan F. D., 1995, Phys. Rev. D, 52, 5707
Ryan F. D., 1997, Phys. Rev. D, 55, 6081
Schilizzi R. T. et al., 2007, SKA Memo 100, Preliminary Specifications for the Square Kilometre Array. SKA Program Development Office
Shapiro S. L., Teukolsky S. A., 1983, Black Holes, White Dwarfs and Neutron Stars: The Physics of Compact Objects. Wiley-Interscience, New York
Shklovskii I. S., 1970, SvA, 13, 562
Silverman J. M., Filippenko A. V., 2008, ApJ, 678, L17
Simonetti J. H., Kavic M., Minic D., Surani U., Vijayan V., 2011, ApJ, 737, L28
Sipior M. S., Portegies Zwart S., Nelemans G., 2004, MNRAS, 354, L49
Smits R., Kramer M., Stappers B., Lorimer D. R., Cordes J., Faulkner A., 2009, A&A, 493, 1161
Smits R., Tingay S. J., Wex N., Kramer M., Stappers B., 2011, A&AS, 528, A108
Thorne K. S., 1980, Rev. Mod. Phys., 52, 299
Thorne K. S., Price R. H., Macdonald D. A., 1986, Black Holes: The Membrane Paradigm. Yale Univ. Press, New Haven
van den Heuvel E. P. J., 1992, in van den Heuvel E. P. J., Rappaport S. A., eds, X-ray Binaries and Recycled Pulsars. Kluwer, Dordrecht, p. 233
Verbiest J. P. W. et al., 2009, MNRAS, 400, 951
Voss R., Tauris T. M., 2003, MNRAS, 342, 1169
Wex N., 1995, Class. Quantum Gravity, 12, 983
Wex N., 1998, MNRAS, 298, 67
Wex N., Kopeikin S., 1999, ApJ, 513, 388
Wex N., Liu K., Eatough R. P., Kramer M., Cordes J. M., Lazio T. J. W., 2013, in van Leeuwen J., ed., Proc. IAU Symp. 291, Neutron Stars and Pulsars: Challenges and Opportunities after 80 years. Cambridge Univ. Press, Cambridge, p. 171
Will C. M., 1993, Theory and Experiment in Gravitational Physics, Cambridge Univ. Press, Cambridge
Yue Y., Li D., Nan R., 2013, in van Leeuwen J., ed., Proc. IAU Symp. 291, Neutron Stars and Pulsars: Challenges and Opportunities after 80 years. Cambridge University Press, Cambridge, p. 577
Yungelson L., Portegies Zwart S. F., 1998, preprint (arXiv:astro-ph/9801127)
Ziółkowski J., 2008, Chin. J. Astron. Astrophys. Suppl., 8, 273

This paper has been typeset from a TEX/LATEX file prepared by the author.